Physics at a 10^{36} Asymmetric B Factory *

The physics opportunities at an asymmetric B Factory operating at the unprecedented luminosity of $10^{36}\mathrm{cm}^{-2}\mathrm{s}^{-1}$ are unique and attractive. The accelerator appears to be practical and the challenges of performing a sensitive experiment in this environment can be met.

Executive Summary

The physics of flavor is central to our understanding of the structure of matter. Recent developments in the quark and neutrino sectors have deepened our understanding of the Standard Model and pointed the way to further experimental studies in the search for new physics. This note presents a first look at the future of the physics of quarks produced in e^+e^- annihilation, at the $\Upsilon(4S)$ and $\Upsilon(5S)$, over the next decade and beyond. We explore the physics case for a very high luminosity asymmetric B Factory, present an initial parameter list of such a machine at a luminosity of $10^{36}\mathrm{cm}^{-2}\mathrm{s}^{-1}$ and explore design considerations for a detector capable of doing new physics at this luminosity. We include very preliminary schedule and cost estimates for the accelerator and detector.

The search for new physics in the flavor sector involves direct searches for new particles (*e.g.* squarks or sleptons), precise tests of Standard Model predictions for rare decay branching fractions and decay distributions and overconstrained tests of the CKM matrix. A very high luminosity asymmetric B Factory can make unique contributions to these studies, as well as providing capabilities complementary to those of experiments at hadronic machines.

The discovery of new SUSY particles will perforce add new amplitudes to loop-mediated flavor decay processes. These can modify rates and angular distributions in rare B decays. The presence or absence of a pole in the $m^2_{l^+l^-}$ distribution in $B^0 \to K^* l^+ l^-$ decay is a striking case in point. These additional amplitudes can also modify $B^0\bar{B}^0$ mixing, thereby changing the pattern of *CP*-violating asymmetries observed in B^0 decays.

Precision tests of CKM unitarity require the percent-level precision on the measurement of $\sin 2\beta$ obtainable at a 10^{36} asymmetric B Factory as well as the several percent precision obtainable on $\sin 2\alpha$ and γ with very large samples of rare hadronic B decays. In particular, measurements of the separate branching ratios of $B^0 \to \pi^0\pi^0$ and $\bar{B}^0 \to \pi^0\pi^0$ decays, possible only at an e^+e^- B Factory, are crucial towards obtaining a precise value of α with theoretical uncertainties. Taken together with concomitant improvements in our understanding of the magnitudes of CKM matrix elements, which require new techniques involving tagging and exclusive reconstruction of B semileptonic decays as well as anticipated improvements in lattice gauge calculations, this program is capable of tests of CKM unitarity of exquisite precision.

Building a 10^{36} asymmetric B Factory requires a substantial extension from existing storage rings, but appears to be feasible with existing techniques. The machine would use the existing PEP tunnel and infrastructure, would retain approximately one half of the present magnets and would extend the existing 476 MHz RF system (with the addition of storage cavities) to cope with the very high beam currents involved. New welded vacuum chambers would be required for both rings. With the luminosity lifetime primarily determined by the collisions themselves, continuous injection would be required. A self-consistent parameter list for this regime has been developed. Given the relative newness of the 10^{36} concept, it is to be anticipated that further work over the next several years will result in substantial refinement of the design and techniques, and some of the areas in which R&D is needed are described in this document.

Doing a precision experiment at a 10^{36} asymmetric B Factory requires a new detector to cope with backgrounds and radiation levels. Initial studies indicate that this is a tractable problem. A detector based on an all silicon tracking detector, and using short radiation length crystals, would be more compact than *BABAR* for example. The higher physics and background rates are dealt with by employing detector systems with high segmentation and short integration times, such as pixel devices and fast scintillating crystals. A variation of the open trigger traditionally employed in e^+e^- experiments appears to be quite practical. For detector readout, techniques pioneered for the new generation of experiments at the Tevatron and LHC appear to be generally applicable to a 10^{36} e^+e^- storage ring.

In summary, the physics case for a 10^{36} asymmetric B Factory appears to be quite strong. The program studied here has many unique aspects and is quite complemen-

*Work supported by Department of Energy contract DE–AC03–76SF00515.

tary to the programs at hadronic machines. The details of machine and detector design are far from mature, but both machine and detector appear to present reasonable challenges. Undoubtedly, developments in both theory and experiment over the next sevreal years will sharpen our vision and allow a clearer determination of the importance of pushing flavor physics investigations to this new level in rare decays and precision measurements.

Introduction

The new asymmetric B factories have now produced the first evidence for *CP* violation in the B meson system. This discovery required unprecedented data samples, which were provided in record time by both the PEP-II and KEK-B colliders. PEP-II now runs above its design luminosity of $3 \times 10^{33}\mathrm{cm}^{-2}\mathrm{s}^{-1}$; KEK-B above $4 \times 10^{33}\mathrm{cm}^{-2}\mathrm{s}^{-1}$. Both colliders have already produced integrated luminosities in excess of 30 fb^{-1}. The groundbreaking *CP* violation measurements are but the first results of a comprehensive program of flavor physics studies that promises further landmark measurements. Planning for upgrades to both the PEP-II and KEK-B B Factories is already well advanced. These modifications will raise the luminosity of these machines beyond 10^{34}. PEP-II has definite upgrade plans in place that will yield a data sample of 600 fb^{-1} in 2007. A wealth of exciting physics will doubtless emerge from this sample.

The search for new physics through extensions of the Standard Model in the quark sector encompasses several distinct approaches:

- The direct search for production of squarks or other new heavy particles at high energy colliders,
- The search for effects of new physics on rare, loop-mediated K, D and B decay rates and angular distributions, and
- The search for deviations from predictions of overconstrained measurements in precision measurements of the Unitarity Triangle.

Exploration using all three complementary approaches will be required to arrive at a full understanding of new physics in the flavor sector. We will discuss the effect of new physics on rare decays and on precision measurements of CKM parameters, both of which are well-suited to exploration with high statistics samples of B and D decays that can be obtained in e^+e^- annihilation in the 10 GeV region.

To achieve these sensitivities in tests of the Standard Model and in searches for the effect of new physics in the flavor sector requires far larger B physics samples than can be produced over the life of PEP-II and KEK-B. These will in part come from the new generation of hadronic experiments at Fermilab and CERN. The unique characteristics of B meson samples produced at the $\Upsilon(4S)$ and $\Upsilon(5S)$ resonances in e^+e^- annihilation provide a unique and complementary approach to physics at this level of sensitivity.

Such samples require an asymmetric B Factory running at the unprecedented luminosity of $10^{36}\mathrm{cm}^{-2}\mathrm{s}^{-1}$, producing 2×10^{10} B mesons per Snowmass year (10^7 s). The design of such an accelerator has been studied at the recently concluded DPF Snowmass study, as have the physics opportunities with such a sample and the design of a detector to do physics in this challenging environment.

Our consideration of a 10^{36} asymmetric B Factory began in the Spring of 2001. An upgrade of this scale requires time to explore technical problems, define and carry out the needed R&D, and refine its physics objectives. It must also, manifestly, be considered in the context of our unfolding understanding over the next several years.

We describe herein the physics potential of a 10^{36} machine, discuss the parameters of a generic collider, consider design considerations for appropriate detector parameters, and list areas in which R&D is required. We conclude with a scenario for the time scale in which the 10^{36} asymmetric B Factory could become an important component of the US HEP program.

Physics Motivation

THE PRECISION OF CKM MATRIX ELEMENTS

A primary goal of the next generation of flavor physics experiments is to perform the most stringent possible tests of the quark sector of the Standard Model. Such tests are conveniently summarized in the Unitarity Triangle construction. *CP*-violating asymmetries now provide a new class of tests of the CKM matrix. The tests involve comparison of unitarity triangle constructions using combinations of sides and angles of the triangles, the sides being determined by measurements of the magnitudes of CKM matrix elements, primarily from absolute rates of semileptonic decays of heavy quarks and from B^0_d and B^0_s mixing. Even at current experimental precision, theoretical uncertainties are a significant limitation on the precision of such tests.

The production of new very large samples of B mesons produced at the $\Upsilon(4S)$ resonance will result in very significant improvements in the precision of semileptonic decay and B^0 mixing measurements, as well as the introduction of improved techniques such as overconstrained reconstruction of semileptonic decay Dalitz plots in recoil spectra. At the same time, improvements in theoretical calculations, primarily lattice gauge solutions of QCD, coming largely from improvements in algorithms

and computational power, will significantly reduce theoretical uncertainties.

The rates at which experimental and theoretical precision improve are uncorrelated. It is worth asking, however, whether improvements over the next decade in the two areas will occur at commensurate rates. It would be less than ideal were the precision of semileptonic branching ratio and mixing measurements to improve so much that theoretical uncertainties were to become completely dominant. It would similarly be less than ideal were theoretical uncertainties in lattice gauge calculations to improve very much more rapidly than experimental precision. The latter is the less likely scenario.

Table I shows the expected precision in absolute semileptonic branching ratio and mixing measurements, as they pertain to the magnitude of various CKM matrix elements, at three values of integrated luminosity: the present, in 2002-2007, when data samples should total 500 fb^{-1}, and in 2003-2011, when data samples in e^+e^- could exceed 10 ab^{-1}. It also, for comparison, shows a prediction, due to Kronfeld, of the expected precision of the relevant lattice gauge theory quantity at the same points in time.

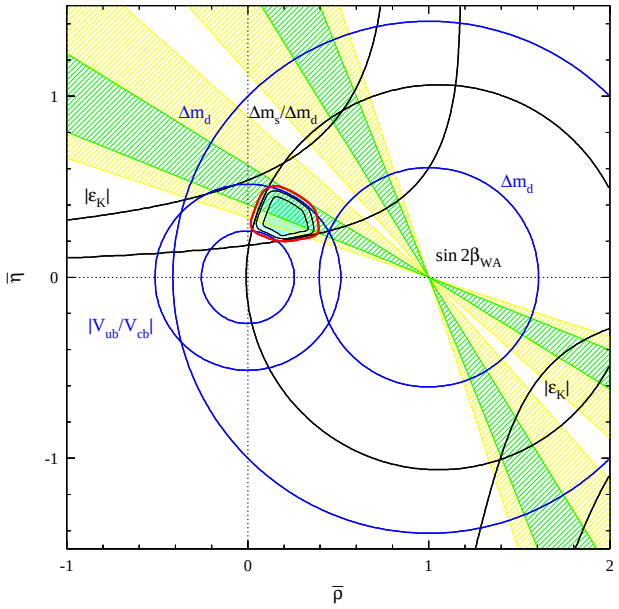

FIG. 1: Allowed region in the $\bar{\rho}-\bar{\eta}$ plane from Höcker *et al.*[3], with the world average of $\sin 2\beta$ including the recent results from *BABAR* and BELLE.

MEASUREMENTS OF UNITARITY ANGLES

Measurement of $\sin 2\beta$

The *BABAR* experiment has recently announced a measurement of *CP* violation in the neutral B meson system, finding $\sin 2\beta = 0.59 \pm 0.14(\text{stat.}) \pm 0.05(\text{syst.})$[1]. Also, the BELLE experiment finds $\sin 2\beta = 0.99 \pm 0.14(\text{stat.}) \pm 0.06(\text{syst.})$[2]. These results are consistent with the expectations from the CKM picture, as shown in Figure 1, but are not yet accurate enough to greatly reduce the allowed region in the $\bar{\rho} - \bar{\eta}$ plane. Future, highly precise, measurements of $\sin 2\beta$ will allow a correspondingly precise test of the CKM model.

The current *BABAR* results can be used to estimate the uncertainty achievable with larger data sets. We extrapolate using just the $B \to J/\psi K_s$, $\psi(2S)K_s$, $\chi_{c1}K_s$ data, which has a statistical uncertainty of 0.015 for roughly 30.5 fb^{-1}. The uncertainty scales as $1/\sqrt{\mathcal{L}}$, so we infer $\sigma_{\sin 2\beta} = 0.037$ for 500 fb^{-1}, and $\sigma_{\sin 2\beta} = 0.008$ for 10 ab^{-1}. These extrapolations assume that the reconstruction efficiency and flavor tagging remains the same.

The systematic error in the current *BABAR* measurement is 0.05, of which 0.03 is due to the Δt measurement, 0.03 due to the flavor tagging, and 0.015 due to the uncertainty in τ_B and Δm_d. At the level of precision possible with either $500 fb^{-1}$ or $10 ab^{-1}$, these systematic effects become significant. Since the flavor tagging is taken from data, it is likely that its uncertainty improves as $1/\sqrt{\mathcal{L}}$. Also with large data samples, the uncertainty in τ_B and Δm_d should significantly improve. Most likely the limiting systematic uncertainty in $\sin 2\beta$ will be due to the Δt measurement. Much of *BABAR*'s present uncertainty comes from the internal alignment of the SVT and it seems quite possible that the uncertainty here can be reduced to less than 0.01. In total we expect a systematic uncertainty of the order of the statistical uncertainty at 10 ab^{-1}.

A measurement of $\sin 2\beta$ with an accuracy better than 0.01 will likely provide the best constraint in the $\bar{\rho} - \bar{\eta}$ plane, and therefore the benchmark for tests of the CKM picture.

Comparison of $\sin 2\beta$ in other decay modes

A comparison of the asymmetry in the pure penguin $b \to s\bar{s}s$ decay $B \to \phi K_s$ with the asymmetry in $b \to c\bar{c}s$ decays is sensitive to new particles with complex couplings. This decay has now been observed[4]; *BABAR* sees roughly 11 events in 22 fb^{-1}. Using the results from the $\sin 2\beta$ measurement, and scaling from the 11 observed events, gives an estimated uncertainty in the ϕK_s asymmetry of $\sigma_{A_{\phi K_s}} = 0.25$ for 500 fb^{-1} and $\sigma_{A_{\phi K_s}} = 0.056$ for 10 ab^{-1}. At these levels systematic uncertainties will remain unimportant. A comparison of the asymmetry between $b \to c\bar{c}s$ and $b \to s\bar{s}s$ at the 0.06 level will be a very powerful probe of new physics appearing in loop diagrams.

The asymmetry in the Cabibbo suppressed decay $B \to$

V_{ij}	Experimental Measurement	σ 2001 stat/sys	σ 2006 stat/sys	σ 2011 stat/sys	Theoretical Quantity	σ 2001 quenched	σ 2-5 years unquenched	σ 4-10 years unquenched
V_{ub}	$B(B \to \rho l\nu)$	4.3%/8%	8.6%/2.4%	1.4%/2.4%	$f_+(E_\pi)$	18%	15%	5%
	$B(B \to u l\nu)$	3.4%/16%	4.0%/2.4%	2.8%/2.4%	f_B †	10-15%	10%	2%
	$B(B \to \tau\nu)$		24%	5%	$\overline{\Lambda}$, λ_1, $\lambda_2'^\star$	see note	see note	see note
V_{cb} $(\mathcal{F}(1))$	$B(B \to D l\nu)$	3.1%/4%	0.4%/2%	0.10%/1%	$\mathcal{F}(1)$ ‡	2-4%	2-4%	1%
V_{cb}	$B(B \to c l\nu)$	2.5%/2%	0.3%/1%	0.07/0.5%%	$\overline{\Lambda}$, λ_1, $\lambda_2'^\star$	25%	15%	5%
V_{us}	$B(K \to \pi l\nu)$	0.8%	0.8%	0.8%	$f_+(q^2)$	15%	15%	2-5%
V_{cd}	$B(D \to \pi l\nu)$	7.1%	1%		$f_+(E_\pi)$	15%	15%	2-5%
	$B(D \to l\nu)$		2%		f_D †	10-15%	10%	2%
V_{cs}	$B(D \to K l\nu)$		0.4%		$f_+(E_K)$	15%	15%	2-5%
	$B(D_s \to l\nu)$		1%		f_{D_s} †	10-15%	10%	2%
V_{td}	Δm_d	1%/1%	0.2%/0.5%	0.05%/0.2%	$f_{B_d}\sqrt{B_{B_d}}$ ♯	∼20%	15%	5%
V_{ts}	Δm_s				$f_{B_s}\sqrt{B_{B_s}}$ ♯	∼20%	15%	5%

† 50% of the error on f_B/f_{D_s}
⋆ from experiment: λ_2 from $m_{B^*} - m_B$; $\overline{\Lambda}$ and λ_1 from moments of $B \to c l\nu$ and $B \to s\gamma$ spectra
‡ lattice measures $\mathcal{F}(1) - 1$
♯ $\xi = \frac{f_{B_s}/\sqrt{B_s}}{f_{B_d}/\sqrt{B_d}}$ error divided by 1.5-2

TABLE I: Projections for improvement in the experimental and theoretical contributions to the precision of CKM matrix elements.

$J/\psi\pi^0$ can also be compared against the asymmetry in $b \to c\overline{c}s$ decays. The asymmetry in $b \to c\overline{c}s$ is theoretically clean because the dominant penguin diagrams have the same phase, namely no phase in the Wolfenstein parameterization, as the tree diagrams. There is, however, a small u-quark penguin component which is commonly assumed to be small. This u-quark component can be bounded by the deviation of the asymmetry in $B \to J/\psi\pi^0$ from $B \to J/\psi K_s$. The statistical uncertainty can be estimated from the roughly 13 signal events observed by *BABAR*, in 23 fb^{-1}, giving a statistical uncertainty of $\sigma_{A_{\phi K_s}} = 0.23$ for 500 fb^{-1} and $\sigma_{A_{\phi K_s}} = 0.052$ for 10 ab^{-1}.

Measurement of $\sin 2\alpha$

A *CP* violating asymmetry can be measured in the decay mode $B \to \pi^+\pi^-$, although the asymmetry in this case depends both on the CKM angle α and on the competing contribution from penguin diagrams. The measured asymmetry in $\pi^+\pi^-$ is given by

$$\sin 2\alpha_{\rm eff} = \sin\left(2\alpha + 2\delta_{\rm Penguin}\right)$$

The penguin contribution, $\delta_{\rm Penguin}$ can also be found from the measurements of the branching ratios $B^0 \to \pi^0\pi^0$ and $\overline{B}^0 \to \pi^0\pi^0$.

The branching ratio for $B \to \pi^+\pi^-$ has been measured with an average value $(4.4 \pm 0.9) \times 10^{-6}$. Using 31 fb^{-1}, *BABAR* has observed 65^{+12}_{-11} $\pi^+\pi^-$ events, and has made the first measurement of the time-dependent asymmetry[5]. The *CP* asymmetry is parameterized as

$$A(\Delta t) = C_{\pi\pi}\cos(\Delta m \Delta t) + S_{\pi\pi}\sin(\Delta m \Delta t)$$

where

$$S_{\pi\pi} = 2\frac{Im\lambda}{(1+|\lambda|^2)} \quad C_{\pi\pi} = \frac{(1-|\lambda|^2)}{(1+|\lambda|^2)}$$

BABAR finds $S_{\pi\pi} = 0.03^{+0.53}_{-0.56} \pm 0.11$, and $C_{\pi\pi} = -0.25^{+0.45}_{-0.47} \pm 0.14$. We estimate the uncertainty for CP asymmetry measurements in $B \to \pi^+\pi^-$ using these results and extrapolating from the number of events found at *BABAR*. We estimate uncertainties of $\sigma_{S_{\pi\pi}} = 0.14$ and $\sigma_{C_{\pi\pi}} = 0.12$ with 500 fb^{-1} and $\sigma_{S_{\pi\pi}} = 0.032$ and $\sigma_{C_{\pi\pi}} = 0.026$ with 10 ab^{-1}. With the precise measurement possible with 10 ab^{-1}, systematic uncertainties from the Δt measurement and backgrounds will be important. Most likely the systematic uncertainties can be kept below the level of the statistical errors.

The $S_{\pi\pi}$ asymmetry can be interpreted in terms of the CKM angle α using the isospin relations among $B \to \pi\pi$ amplitudes[6]. The angle $\delta_{\rm Penguin}$ may be found using the rates of $B^0 \to \pi^0\pi^0$, $\overline{B}^0 \to \pi^0\pi^0$, $B^0 \to \pi^+\pi^-$, $\overline{B}^0 \to \pi^+\pi^-$, and $B^+ \to \pi^+\pi^0$ as shown in the pair of triangles in Figure 2. These triangles are altered slightly by the effect of EW penguin diagrams, but these can be included as a correction. The challenge is to measure the $\pi^0\pi^0$ decay with enough precision to determine the angles of each isospin triangle.

The $\pi^0\pi^0$ decay mode suffers from a high level of background, from $q\overline{q}$ combinatorics. The uncertainty in the

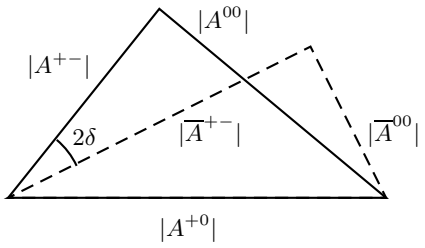

FIG. 2: Isospin triangles for decays $B \to \pi\pi$ and $\overline{B} \to \pi\pi$

branching ratio can be expressed as

$$\sigma_{\mathcal{B}}^2 = \frac{(\mathcal{B} + f\mathcal{B}^{\rm Background})}{\epsilon^{\rm signal} \int \mathcal{L}(nb^{-1})}$$

where f accounts for the statistical precision of the background extrapolation and typically $f \sim 1.13$. The background level is estimated from *BABAR* simulation to be roughly $\mathcal{B}^{\rm Background} = 8 \times 10^{-6}$, where $\mathcal{B}^{\rm Background} = N^{\rm Background}/\epsilon^{\rm signal} \int \mathcal{L}(nb^{-1})$. The isospin construction requires the measurement of the flavor tagged branching ratio. Although the efficiency is reduced by the requirement of a flavor tag, the S/B ratio is significantly improved by this requirement. Using just a lepton tag, with an efficiency of roughly 11%, we conservatively estimate an increase in S/B of a factor of 4. Using a value of $\mathcal{B}^{\rm Background} = 2 \times 10^{-6}$ we can estimate the uncertainty in the determination of the angle $\delta_{\rm Penguin}$ as a function of the value of $\mathcal{B}(B \to \pi^0\pi^0)$ as shown in Figure 3, for a range of integrated luminosities. The uncertainty levels shown do not depend strongly on the values chosen for $B^0 \to \pi^+\pi^-$, $\overline{B}^0 \to \pi^+\pi^-$, or $B^+ \to \pi^+\pi^0$. The uncertainties of the other branching ratios have also been included in the $\delta_{\rm Penguin}$ analysis. The vertical variation in the value of $\sigma(\delta_{\rm Penguin})$ is a function of the value of $\delta_{\rm Penguin}$.

The estimated uncertainty of less than 5^o for $\delta_{\rm Penguin}$ in 10 ab^{-1} translates into an uncertainty in the CKM angle α of less than 5^o, which is somewhat greater than the uncertainty from the $S_{\pi\pi}$ measurement of order 1.6^o. With 10 ab^{-1} the level of uncertainty for α will provide a constraint in the $\bar{\rho} - \bar{\eta}$ plane close to the level of the $\sin 2\beta$ measurement; combined they provide a precise test of the CKM picture.

Measurement of γ with $B \to DK$

The CKM angle γ can be measured from combinations of the decays $b \to c\overline{u}s$ and $b \to u\overline{c}s$, where the former decay has no weak phase, and the latter decay has weak

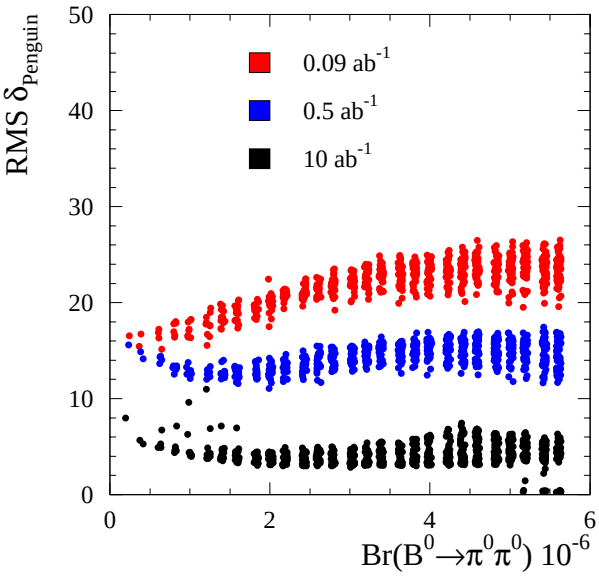

FIG. 3: Uncertainty in the Penguin angle $\delta_{\rm Penguin} = \alpha_{\rm Eff} - \alpha$ in degrees vs. the branching ratio $\mathcal{B}(B \to \pi^0\pi^0)$ for $90fb^{-1}$, $500fb^{-1}$, and $10ab^{-1}$.

phase γ. Gronau and Wyler suggested[7] that the relations

$$\sqrt{2}A(B^+ \to D_1^0 K^+) = A(B^+ \to D^0 K^+) + A(B^+ \to \overline{D}^0 K^+)$$

and its CP conjugate could be used to determine γ. Here $D_1^0 = \frac{1}{\sqrt{2}}(D^0 + \overline{D}^0)$, is a CP eigenstate. However, Atwood, Dunietz, and Soni[8] have shown that doubly Cabibbo suppressed $\overline{D}^0$ decays which mimic D^0 decays make the Gronau-Wyler construction difficult to implement. Atwood, Dunietz and Soni went on to demonstrate that $B \to DK$ decays, using at least two different D^0 decays which are not CP eigenstates, could be used to extract γ. In this construction, four relations of the type

$$\mathcal{B}(B^- \to K^- f_i) = \mathcal{B}(B^- \to K^- D^0)\mathcal{B}(D^0 \to f_i) + \mathcal{B}(B^- \to K^- \overline{D}^0)\mathcal{B}(\overline{D}^0 \to f_i) + 2\cos(\xi_i + \gamma) \times \sqrt{\mathcal{B}(B^- \to K^- D^0)\mathcal{B}(B^- \to K^- \overline{D}^0)\mathcal{B}(D^0 \to f_i)\mathcal{B}(\overline{D}^0 \to f_i)}$$

and its conjugates, are used to determine $\mathcal{B}(B^- \to K^-\overline{D}^0)$, the strong phase shifts ξ_1 and ξ_2, and γ. Of course, theses types of construction suffers from an eight-fold ambiguity in the value of γ, so high precision is necessary to separate the multiple solutions for γ.

A recent study[9] by Soffer of the precision possible in a measurement of γ used both the Gronau-Wyler and Atwood-Dunietz-Soni $B \to DK$ constructions, and the

decay modes $f_i = K^-\pi^+, K^-\pi^+\pi^0, K^-\pi^+\pi^-\pi^+$. In addition, all possible D or D^* and K or K^* combinations were included. The Soffer study solved for γ using a χ^2 minimization for the various branching ratio measurements. The χ^2 result, as a function of γ, for $600 fb^{-1}$ is shown in Figure 4, for four possible sets of values of both γ and the strong phases. Typically the error on γ is $\sigma_\gamma \sim 5^\circ - 10^\circ$ for a particular solution for γ. However, the χ^2 distribution shows that combining a range of two or three sigma around each solution covers much of the possible range for γ, such that a data sample of $600 fb^{-1}$ does not really allow a determination of γ.

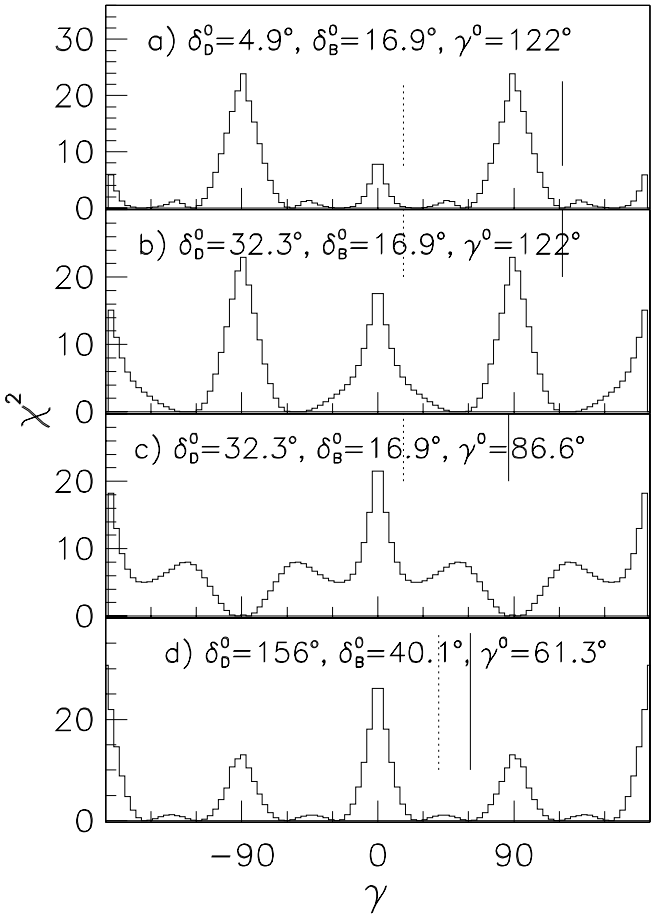

FIG. 4: χ^2 as a function of trial values of γ, minimized with respect to the strong phase shifts δ_B, δ_D, and the ratio r of the Cabibbo suppressed process to the Cabibbo allowed process at each point. The integrated luminosity simulated is 600 fb^{-1}.

With a luminosity of $10 ab^{-1}$ the situation will be qualitatively different, and the CKM angle γ will be well measured using decays $B \to DK$. The χ^2 inferred in the Soffer study can be scaled by a factor proportional to the luminosity. In this case, the statistical uncertainty improves to the $\sigma_\gamma \sim 1^\circ - 2.5^\circ$ level for individual solutions, and some ambiguities may be removed using several $B \to DK$ decay modes. Also at this level of precision, it will be possible to identify the solution of interest from other CKM angle measurements.

Measurement of sin(2β + γ)

The combination of CKM angles $2\beta + \gamma$ can be measured in decays of the type $B \to Dh$, where h is a π, ρ, or other meson. Several strategies for measuring the combination $2\beta + \gamma$ have been proposed[10], all of which utilize the interference between $b \to c\overline{u}d$ and B mixing followed by $\overline{b} \to \overline{u}c\overline{d}$, where the latter process depends on the angle γ.

Initially, Aleksan, Dunietz, and Kayser suggested that the decay $B \to D^{*+}\pi^-$ be used. The large branching ratio, roughly 0.28%, offsets the small asymmetry expected. However, this method suffers from the necessity to also measure the ratio, r, of the doubly Cabibbo suppressed decay $\overline{b} \to \overline{u}c\overline{d}$ and the dominant decay $b \to c\overline{u}d$. A recent study[11] for *BABAR* considered both fully reconstructed decays and partially reconstructed decays. Extrapolating from that study gives estimates for the uncertainty at $\sigma_{\sin(2\beta+\gamma)} \sim 0.15$ for 500 fb^{-1} and $\sigma_{\sin(2\beta+\gamma)} \sim 0.03$ for 10 ab^{-1}. The probability that the r ratio is not measurable due to statistical fluctuations is roughly 15% with 500 fb^{-1}, and roughly 3% with 10 ab^{-1}.

Recently, London, Sinha and Sinha[12] have proposed an analysis using vector mesons, such as the decay $B \to D^*\rho$, with a time-dependent angular analysis. In this case the small ratio of doubly Cabibbo suppressed decays to the dominant decay is more easily measured, improving the statistical precision possible in the measurement of $\sin(2\beta + \gamma)$. This technique awaits a more complete numerical analysis, but may be quite promising.

Diehl and Hiller [13] attempted to overcome the problems in the $B \to D^*\pi$ modes by using light hadrons $h^\pm$ which have a suppressed decay constant, and thus couple very weakly to the $W^\pm$. For the lightest such hadron, a_0^+, they estimate the branching fraction $Br(B^0 \to D^{(*)-}a_0^+) \sim (1-4) \times 10^{-6}$. Since a_0^+ decays to $\pi^+\eta$, it is possible to estimate the signal and background rates from the *BABAR* measurement of $B \to D^{(*)\mp}\rho^\pm$. We thus find that in 10 ab^{-1} one may expect $30 - 140$ signal events, with no less than 3500 background events. We conclude that this mode could perhaps provide a useful cross-check for $\sin(2\beta + \gamma)$ if one uses all the decay constant-suppressed mesons possible.

PHYSICS AT THE $\Upsilon(5S)$

Strategies using B_s^0 decays require PEP-II to operate at the $\Upsilon(5S)$ resonance. A dedicated $\Upsilon(5S)$ run will probably have a lower priority than the $\Upsilon(4S)$, but physics

with B_s^0 mesons offers interesting and complementary opportunities to the study of B_d^0 decays. Although traditional CP violating studies via time-dependent asymmetries will be very difficult in the B_s^0 system due to limited vertex resolution there are new and promising techniques that only require time-integrated measurements or moderate time resolution. In the following, we will first give a brief introduction to the $\Upsilon(5S)$ resonance and then discuss the strategies to measure γ at the $\Upsilon(5S)$.

The parameters of the $\Upsilon(5S)$ resonance have been determined by a previous CESR run: $M(5S) = (10866 \pm 20)$ MeV, $\Gamma(5S) = (101 \pm 13)$ MeV, and $\Gamma_{ee}(5S) = (0.30 \pm 0.04)$ KeV [14]. Also the energy dependence of the total cross-section above the $\Upsilon(4S)$ has been measured [15]. However, the $\Upsilon(5S)$ can decay into pairs of $\mathrm{B_u}, \mathrm{B_d}, \mathrm{B_s}$ + c.c. and $\mathrm{B_u^*}, \mathrm{B_d^*}, \mathrm{B_s^*}$ + c.c. mesons, obeying flavor-conservation. These individual cross sections have not been measured yet. It is a commonly used assumption that the B_s^0 related cross section consisting of $B_s^0\,\bar{B}_s^0$, $B_s^*\,\bar{B}_s^0 + B_s^0\,\bar{B}_s^*$ and $B_s^*\,\bar{B}_s^*$ is 1/3 of the total $\Upsilon(5S)$ cross-section, or 0.1 nb. This is approximately 1/10 of the total $\Upsilon(4S)$ rate. The assumption is in agreement with a coupled-channel model analysis of the total cross-section [15], the observation of Doppler-broadened monochromatic photons from B_s^* decays [14], and the reconstruction of B_s^0 decay products in the CLEO detector [16]. With 0.1 nb inclusive B_s^0 cross-section, an integrated luminosity of 100 fb^{-1} yields 10^7 $B_s^0\,\bar{B}_s^0$ pairs, and 1 ab^{-1} 10^8 $B_s^0\,\bar{B}_s^0$ pairs, respectively.

Measuring γ at the $\Upsilon(5S)$

A key role in the determination of γ in B_s^0 decays is played by exclusive B_s^0 decays originating from quark transitions $\bar{b} \to \bar{u}c\bar{s}$ and $b \to c\bar{u}s$. Examples are decays as $D_s^{\pm}\,K^{\mp}$, $D_s^{*\pm}\,K^{\mp}$, $D_s^{\pm}\,K^{*\mp}$ and $D_s^{*\pm}\,K^{*\mp}$, with branching ratios of $\mathcal{O}(10^{-4})$ expected for each mode. From a theoretical point of view, these modes are very similar to $\mathrm{B_d^0} \to \mathrm{D^{*\pm}}\pi^{\mp}$ discussed in the previous section, and allow us (in principle) to extract the observables $\lambda(B_s^0 \to f)$ and $\lambda(B_s^0 \to \bar{f})$. The important difference is that both decay paths are equally CKM-suppressed in the B_s^0 case, and the $B_s^0\,\bar{B}_s^0$ mixing phase is tiny within the Standard Model. From an experimental point of view, the extraction of $\lambda(B_s^0 \to f)$ and $\lambda(B_s^0 \to \bar{f})$ from the data is completely different than in the $\mathrm{B_d^0} \to \mathrm{D^{*\pm}}\pi^{\mp}$ case. Flavor-tagged time-dependent asymmetries cannot be resolved for B_s^0 mesons due to very rapid $B_s^0\,\bar{B}_s^0$ oscillations. An alternative is provided by the expected sizeable width difference $y_s = \Delta\Gamma/2\Gamma$ between the two mass eigenstates. Because of the width difference, *untagged* data samples of $B_s^0 \to D_s^{(*)\pm}\,K^{(*)\mp}$ are sufficient to determine γ. In such untagged B_s^0 decays rates, the rapid oscillatory $\Delta m_s \Delta t$ terms cancel, and the time evolution is governed by two exponentials with a γ-dependent interference term. The formulas for the time-dependent decay rate of untagged B_s^0 mesons at the $\Upsilon(5S)$ are given in Ref. [17]. These decay time distributions can be understood as corrections to the exponential decay distribution $\propto e^{-|\Gamma\Delta t|}$ in powers of y_s. For B_s^0 flavor states ($\lambda = 0$) there are only second order terms in y_s, whereas CP eigenstates ($|\lambda| = 1$) or any other states with interfering amplitudes ($0 < |\lambda| < 1$) have first order terms in y_s. Important for the measurement of CP phases is the fact that the first order terms in y_s scale with a factor proportional to $\mathrm{Re}(\lambda)$. In general it is found, that any measurement of CP phases that relies on the oscillation parameter $x_s = \Delta m_s/\Gamma$, determines $\mathrm{Im}(\lambda)$ whereas a measurement that makes use of y_s determines $\mathrm{Re}(\lambda)$.

One important property at the $\Upsilon(5S)$ is that $B_s^0\,\bar{B}_s^0$ pairs may be produced in a symmetric ($C = 1$) or anti-symmetric ($C = -1$) wavefunction. The former case occurs for $B_s^*\,\bar{B}_s^0 + B_s^0\,\bar{B}_s^*$ production, the latter for $B_s^0\,\bar{B}_s^0$ and $B_s^*\,\bar{B}_s^*$. Emission of a photon in $\mathrm{B_s^*} \to \mathrm{B_s^0}\gamma$ changes the sign of the C-parity. In the following the fraction of C-odd produced $B_s^0\,\bar{B}_s^0$ pairs is labeled as $R_{\pm}$:

$$R_{\pm} = \frac{f(\eta_c = -1)}{f(\eta_c = -1) + f(\eta_c = +1)} \; . \qquad (1)$$

For an illustration of the statistical accuracy to be expected for γ, Fig. 5 shows the 1σ statistical error on γ in a hypothetical measurement with $\gamma = 90^0$ for data samples of 1,000 and 10,000 reconstructed $D_s^{(*)\pm}\,K^{(*)\mp}$ events. The statistical error is shown as a function of three, at present, only poorly known parameters: y_s, the normalized decay width difference, $R_{\pm}$, the fraction of C-odd produced $B_s^0\,\bar{B}_s^0$ pairs, and $|\lambda|$, the magnitude of interfering amplitudes in $D_s^{(*)\pm}\,K^{(*)\mp}$. The theoretical estimate for y_s is 0.075 ± 0.035 [18], $R_{\pm}$ is unknown and can vary in the range from 0 to 1, and $|\lambda|$ is expected in the range [19] $|\lambda| = 0.36 \pm 0.08$. All three parameters will be determined by independent measurements and will enter as fixed parameters in the time-dependent fit. Reconstruction of the C state in the event is not required, only the value of $R_{\pm}$ has to be known. The estimated error is the purely statistical error, while systematic uncertainties or background have not been considered. The number of reconstructed events is derived for a luminosity of 100 fb $^{-1}$ and 1 ab $^{-1}$, respectively. This estimate is based on a B_s^0 cross-section of 0.1 nb and partial reconstruction of $D_s^{(*)\pm}\,K^{(*)\mp}$ decays with typical *BABAR* reconstruction efficiencies. Such partial reconstruction techniques can be applied for the $D_s^{*\pm}\,K^{\mp}$ mode, similar to $\mathrm{B_d^0} \to \mathrm{D^{*\pm}}\pi^{\mp}$ at the $\Upsilon(4S)$, where only the photon from the $\mathrm{D_s^*}$ and the $K^{\mp}$ are reconstructed. Also, in case of B_s^* production, the photon from $\mathrm{B_s^*} \to \mathrm{B_s^0}\gamma$ may be exploited for partial reconstruction. With the γ from B_s^* , and a reconstructed $K^{\mp}$ or $K^{*\mp}$, the missing momentum can be used to estimate the unmeasured $D_s^{(*)\pm}$. As can be seen in Fig. 5, values of y_s below 0.08 are still very

critical for a measurement based on 1,000 events, but acceptable with a statistics of 10,000 events.

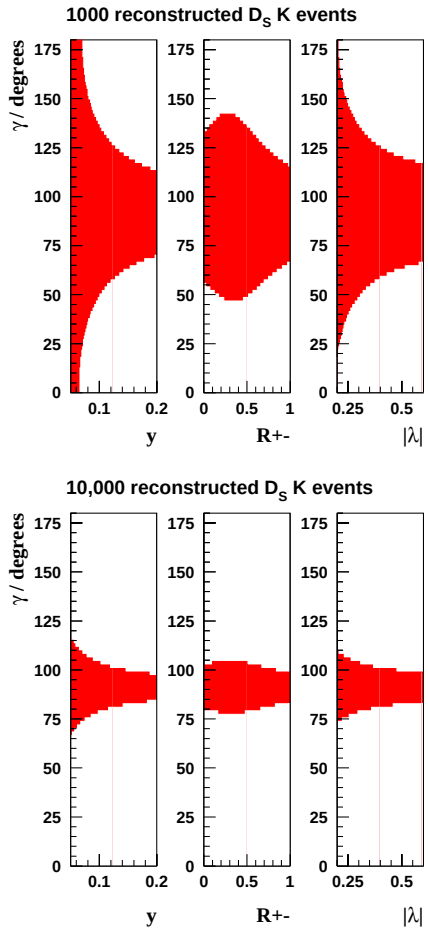

FIG. 5: The statistical resolution on γ is shown as a function of y_s, $R_\pm$ and $|\lambda|$ for 1,000 and 10,000 $D_s^{(*)\pm}\,K^{(*)\mp}$ events. The hypothetical measurement, based on 100 fb^{-1} and 1 ab^{-1} of data, respectively, assumes a central value of $\gamma = 90^0$.

New Physics at the $\Upsilon(5S)$

CP violation in B_s^0 - $\bar{B}_s^0$ mixing is a prime candidate for the discovery of physics beyond the Standard Model. In the Standard Model the B_s^0 mixing phase is close to zero, and is very sensitive to New Physics. While such new contributions are likely to also affect B_d^0 - $\bar{B}_d^0$ mixing, they appear in the B_d^0 system as corrections to the Standard Model prediction for the angle β. Since the value for β will always involve experimental and theoretical uncertainties, a much stronger test can be made for the B_s^0 system where any non-zero CP phase is a clear and unambiguous signal for New Physics.

A measurement of the B_s^0 mixing phase can be performed by a quantitative comparison of the y_s value measured in semileptonic B_s^0 decays with the one measured in CP eigenstates such as $J/\psi\,\phi$ and $D_s^\pm\,D_s^\mp$. Whereas semileptonic decays have only second-order dependence on y_s and are unaffected by the presence of New Physics, CP eigenstates have linear terms in y_s and are sensitive to a possible New Physics phase Φ. New Physics will appear as an inconsistency in the y_s measurements in semileptonic and CP eigenstates. In first approximation, while assuming $\Phi = 0$, y_s measured in $J/\psi\,\phi$ and $D_s^\pm\,D_s^\mp$ would be smaller by a factor of $\cos\Phi$ than the y_s value measured in semileptonic decays. For a measurement of Φ, one will first measure y_s in semileptonic decays, then constrain y_s to this value in CP eigenstates and fit for $\cos\Phi$.

The accuracy at which $\cos\Phi$ can be measured is very promising with a modest luminosity of 100 fb^{-1}. Fig. 6 shows the 1σ statistical error for y_s in 50,000 reconstructed semileptonic and 3,000 reconstructed CP eigenstates as a function of $R_\pm$, the fraction of C-odd produced $B_s^0\,\bar{B}_s^0$ pairs. The error is purely statistical and estimated for a luminosity of 100 fb^{-1} assuming typical *BABAR* efficiencies. The figures show it is reasonable to expect a resolution for y_s of 0.02 (assuming a central value of 0.1) and for most values of $R_\pm$ the resolution is better for semileptonic decays than for CP eigenstates. This means the phase of New Physics could be tested at the level of $\Delta(\cos\Phi)$ between 0.2 and 0.3.

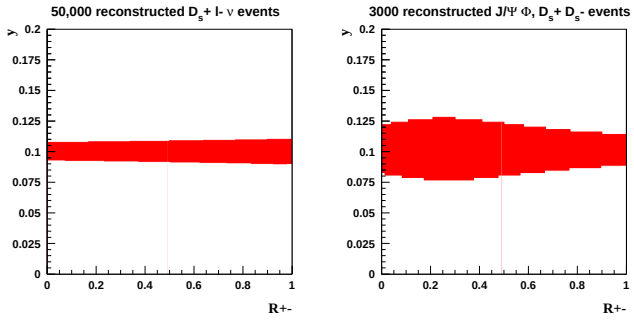

FIG. 6: The statistical resolution on y_s is shown as a function of $R_\pm$ measured in two final states: 50,000 semileptonic and 3,000 $J/\psi\,\phi$ and $D_s^\pm\,D_s^\mp$ events. The hypothetical measurement, based on 100 fb^{-1} of data, assumes a central value of $y_s = 0.1$ and no New Physics phase. In the presence of a new phase in B_s^0 mixing the y_s values measured in semileptonic and CP eigenstates would be different.

SUMMARY OF CKM ANGLE MEASUREMENTS

A summary of the potential of the 10^{36} collider for measurements of the CKM angles is shown in Table II. Comparisons with both BTeV and LHCb are made for these measurements[22].

The 10^{36} collider appears to have the capability to measure all three *CP* violating angles with superb precision. In general, multiple complementary measurements

of the CKM angles are possible, demonstrating the comprehensive B physics program possible at an next generation asymmetric B Factory. In particular, the measurement of the $B^0 \to \pi^0\pi^0$ and $\overline{B}^0 \to \pi^0\pi^0$ rates for a theoretically clean determination of the angle α would be a unique contribution of a 10^{36} collider. Finally, the studies presented here are not an exhaustive list of the physics possibilities; both further study and the measurements made in the next few years at *BABAR* and BELLE will further clarify the physics case for a 10^{36} collider.

B TAGGING

Since the $\Upsilon(4S)$ decays to a pair of B and $\bar{B}$ mesons, if one of the B mesons is fully reconstructed, then all other particles in the event come from the other $\bar{B}$ decay. With this B tagging method, both $q\bar{q}$ continuum and $B\bar{B}$ combinatorial backgrounds can be greatly reduced. At present B-factories, however, B tags have not been used extensively due to the low tagging efficiencies. A 10^{36} B Factory with large B tag samples would open up various opportunities in rare B physics study. For example, detection of the decays, $B \to X_s\nu\bar{\nu}$ or $B \to \tau\nu$, would be hopeless even in the clean environment of e^+e^- production, unless full tagging of the other B can separate the daughter particles of the two B's. With B tags we can also carry out model-independent analysis, for example $B \to X_s\gamma$, where the signal in E_γ distribution is extracted without reconstructing the X_s system.

Full Hadronic Tags

Full reconstruction of B mesons in hadronic channels provides a very clean sample of B tags. Typical decay modes used for full reconstruction are: $B \to D^{(*)} + n\pi$; $D^* \to D+\pi(\text{or }\gamma)$; and $D \to K+m\pi$, where n=1,2,3 and m=1,2,3 . B meson reconstruction efficiency in excess of 0.2% has been achieved by CLEO[23] for the $B^- \to \tau^-\nu$ analysis. The corresponding D^0 reconstruction efficiency was 16%, consistent with *BABAR* estimates [34]. We obtain similar reconstruction efficiencies for neutral B mesons. Therefore, the full hadronic tagging efficiency at higher luminosity B Factory is estimated conservatively at 0.2%. In addition, full reconstruction also provides the momentum vector of the other B, so that daughter particles can be transformed to the true B center-of-mass system, instead of the $\Upsilon(4S)$ center-of-mass system. Any two-body decays of the B then produce sharp peaks in the momentum spectrum of the daughter particles.

Full Semileptonic Tags

Despite the lack of information on the other B momentum vector due to the missing neutrino, semileptonic tags still provide a relatively clean sample. Semileptonic decays of B meson are dominated by two decay modes, $B \to D\ell\nu$ and $B \to D^*\ell\nu$ with branching ratios of 2.2% and 5.0% respectively. Combining the muon and electron modes, roughly 15% of B decays are through these channels. Most analysis at CLEO/*BABAR*/BELLE are limited to clean D decay modes, to reduce the combinatorial background and to minimize systematic uncertainties. Similarly D^* decay modes with π^0 and γ are not used in many analysis. As an example, a *BABAR* analysis of V_{cb} in $B^0 \to D^*e\nu$ decay, obtained a tagging efficiency of 0.13×10^{-4} while using only the $D^0 \to K^-\pi^+$ channel. We can gain a factor of 4 by including other D decay modes as in the hadronic B tags, another factor of 1.8 from the semi-muonic B decay and a smaller gain of 30% from the $D\pi^0$ mode of the D^*. This gives us $D^*\ell\nu$ tagging efficiency of 0.13%. Adding the additional $B \to D\ell\nu$ mode, we estimate the total semileptonic tagging efficiency to be at the 0.2% level.

Partial Semileptonic Tags

B tags in the $D\ell\nu$ mode suffer from large contamination from $D^*\ell\nu$ and $DX\ell\nu$ modes, because the signal in the missing mass spectrum is too broad for clean separation. Instead, we can get a sample of B tags in $DX_{missing}\ell\nu$ mode, with a caveat that there might be a soft pion or a photon left over from the B tag side. They certainly pose no problem for analysis such as $B \to X_s\gamma$. Full semileptonic tags then becomes a subset of the larger partial semileptonic sample. A CLEO analysis of the $B \to D\ell\nu$ branching ratio[24] obtained 0.18% reconstruction efficiency for $D^0X_{missing}\ell\nu$, while using only the $D^0 \to K^-\pi^+$ mode. Including additional D decay modes, we estimate the partial semileptonic tag efficiency of at least 0.6%. Preliminary study at *BABAR* is consistent with this projection [28].

Partial Tags with Missing Charm

Partially tagged B's with missing D's, can also be useful, if the missing particles do not contaminate reconstruction of the other B, which is the case in many pseudo-two-body rare B decay analyses. These tags are not, however, suitable for analyses such as $B \to \tau\nu$.

In hadronic modes, we have $B \to D^*\pi$ or $D^*\rho$ and $D^* \to D\pi$, where the D meson is not reconstructed. The soft pion from D^* decay will be recoiling against the fast π (or ρ) in the B rest frame. CLEO's $B\bar{B}$ mixing analysis [25] with partially reconstructed B's obtained detection

CKM Angle	*BABAR* (0.5 ab^{-1})	Super*BABAR* (10 ab^{-1})	BTeV	LHCb	Atlas/CMS
sin2β ($B^0 \to J/\psi K^0_S$)	0.037	0.008	0.025	0.014	0.021/0.025
sin2β ($B \to \phi K_s$)	0.25	0.056			
sin2α ($B^0 \to \pi^+\pi^-$)	0.14	0.032	0.024	0.056	0.10/0.17
$\alpha_{\rm Eff.} - \alpha$ ($B^0 \to \pi^0\pi^0$)	$< 18^\circ$	$< 7^\circ$	-	-	-
sin $(2\beta + \gamma)$ ($B^0 \to D^*\pi$)	0.15	0.03			
γ ($B \to DK$)	-	$< 2.5^\circ$	$< 10.0^\circ$	$< 19.^\circ$	
γ ($B_s \to D_s K$)	-	$< 15^\circ$	$< 7.0^\circ$	$< 13.^\circ$	

TABLE II: Summary of the estimated precision of CKM angle measurements for both *BABAR* and Super*BABAR*, compared to planned experiments at hadronic colliders. Entries with a dash (−) indicate measurements that cannot be made for a given experiment; blank entries indicate measurements for which no study has yet been made.

efficiencies of 31% and 10% for $D^*\pi$ and $D^*\rho$, respectively. A preliminary study at *BABAR* obtained a similar detection efficiency of 27.5% in the $D^*\pi$ mode [26]. After multiplying them by the appropriate B decay branching ratios and then adding the two modes, we have 0.15% tagging efficiency for partially reconstructed hadronic B's.

CLEO[27] and BABAR[26] have also performed partial reconstruction of the semileptonic $B \to D^*\ell\nu$ decay, where the D meson is not reconstructed. Pseudo missing mass was calculated using the soft pion from the D^* decay and the lepton. The signals were not very clean with an S/B ratio of 1/3. However, the dominant background source was random combinatorics from $B\bar{B}$ events, showing that continuum $q\bar{q}$ background can be effectively suppressed with these tags. CLEO analysis used the partial tagging to study the q^2 distribution in the $D^*\ell\nu$ decay and obtained a tagging efficiency of 0.5%. BABAR analysis on the other hand used the partial tagging to measure the τ_B and the $B\bar{B}$ mixing rate. With more stringent cuts, the tagging efficiency at BABAR was 0.16%.

In summary we assume 0.2% efficiency for a clean sample of B's from full hadronic tagged B's and 1.0% for not so clean B tags. In 0.5(10) ab^{-1} of data, which translates into 2(40) million clean tags and 10(200) million less clean tags, summed over charged and neutral B mesons.

MEASURING V_{ub}

The ratio $|V_{ub}|/|V_{cb}|$ has been measured by CLEO using the detection of inclusive leptons from semileptonic B meson decay beyond the kinematic endpoint for final states containing charm mesons [29]. More recently CLEO was able to reconstruct exclusive transitions, and $|V_{ub}|$ was extracted from the branching fractions of the exclusive transitions [30]. However large theoretical uncertainty ($\sim 20\%$) severely limits the precision of these measurements.

There are two main theoretical approaches to improve the determination of $|V_{ub}|$. The first of these is the operator product expansion (OPE) which is able to predict the inclusive $b \to u\ell\nu$ rate to $5-10\%$ within experimentally tractable regions of phase space (either the region of $m_{\rm had} < m_{\rm D}$ or the endpoint of the q^2 spectrum). The second theoretical approach is lattice QCD (LQCD). There has been a great deal of progress in LQCD in the last few years and within a few years unquenched calculations of the rate for exclusive semileptonic decays will be available. The LQCD calculations may have an error of a few percent or better. Further discussion of the theoretical issues in the extraction of a precision value of $|V_{ub}|$ can be found in [31] [32] [33].

The simulations reported here are for a symmetric e^+e^- B Factory. We use a fast (parametric) Monte Carlo of the CLEO-III detector called TRKSIM with the CLEO $\Upsilon(4S) \to B\bar{B}$ event generator. Efficiencies and S/B for asymmetric B Factories will differ slightly but the general conclusions are likely to be unchanged. Powerful suppression of the $b \to c\ell\nu$ background can be achieved by full reconstruction of the companion B decaying to $B \to D^{(*)}(n\pi)$. As B tagging has a relatively low efficiency of 0.2% [34], the technique was impractical for most analyses with pre-B-factory samples, but will be used extensively in future. We assume 1% systematic error in lepton identification, and 2% systematic error in tracking in the estimates for V_{ub}.

Inclusive hadronic mass spectrum

To minimize both theoretical and experimental systematic effects, the inclusive $b \to u\ell\nu$ process is ideally measured in a fully tagged sample, in which one B is exclusively reconstructed. Then the other B is required to have only one lepton, with momentum greater than 1.4 GeV, and missing mass consistent with a neutrino. We select $b \to u\ell\nu$ events with $m_{\rm had} < m_{\rm D}$. Figure 7(a) shows the simulated $m_{\rm had}$ distribution for an integrated luminosity of 1000 fb^{-1}. Table III shows the estimate of the statistical and systematic error on $V_{\rm ub}$ measured with this method.

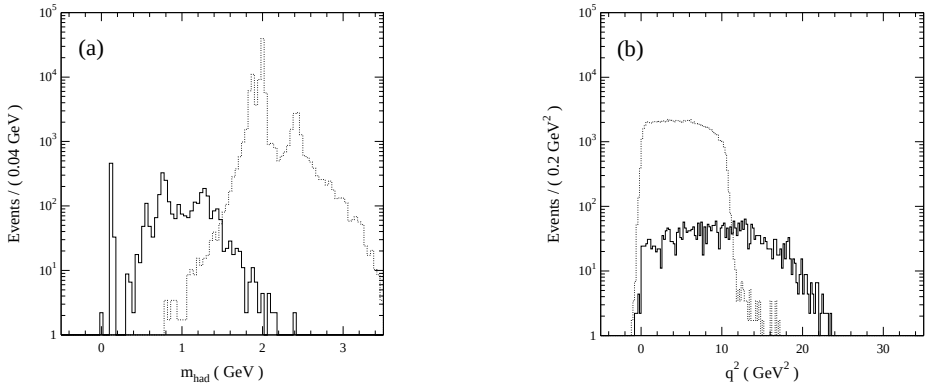

FIG. 7: (a) Hadronic mass ($m_{\rm had}$) distribution for 1000 fb^{-1} data found with CLEO III fast MC. The solid histogram is the $m_{\rm had}$ distribution of $b \to u\ell\nu$, and the dashed histogram is the $m_{\rm had}$ distribution of $b \to c\ell\nu$. (b) q^2 distribution for 1000 fb^{-1} data found with CLEO III fast MC. The solid histogram is the q^2 distribution of $b \to u\ell\nu$, and the dashed histogram is the q^2 distribution of $b \to c\ell\nu$.

method	$\int \mathcal{L}$ fb^{-1}	S	B	$\delta V_{\rm ub}$ (%)		
				stat.	sys.	tot.
$m_{\rm had}$	100	335	127	3.2	2.2	3.9
	500	1675	635	1.5	1.5	2.1
	1000	3350	1270	1.0	1.5	1.8
q^2	100	127	7	4.6	3.0	5.5
	500	635	36	2.0	1.2	2.3
	1000	1270	72	1.4	1.2	1.8
exclusive	1000	590	59	4.3	1.2	4.5
	10000	5900	590	0.7	1.2	1.4

TABLE III: Estimate of the experimental error on $V_{\rm ub}$, using the three methods described in the text. S and B are the number of signal and background events. For $m_{\rm had}$ we assume a 10% uncertainty in B for $\mathcal{L}_{int} = 100 fb^{-1}$, and a 5% uncertainty in B at $\mathcal{L}_{int} \geq 500 fb^{-1}$. For q^2 we assume a 100% uncertainty in B at $\mathcal{L}_{int} = 100\ fb^{-1}$, and a 20% uncertainty in B at $\mathcal{L}_{int} \geq 500\ fb^{-1}$. And for exclusive decays we assume $S/B = 10/1$, and a 10% uncertainty in B for this estimate.

Inclusive q^2 spectrum

Using the inclusive q^2 endpoint results in a loss of statistics, but a gain in theoretical certainty compared to the low $m_{\rm had}$ region. The experimental advantage of this method compared to the $m_{\rm had}$ method is that the S/B is more favorable, therefore this method will be more attractive with very large data samples. B tagging and event selection are the same as in the previous method. We select $b \to u\ell\nu$ events with $q^2 > 11.6$ GeV^2. Figure 7(b) shows the simulated q^2 distribution for an integrated luminosity of 1000 fb^{-1}. Table III shows the estimate of the statistical and systematic experimental errors on $V_{\rm ub}$ obtained with this method for three data samples.

Exclusive decays with Lattice predictions

LQCD aims to predict the decay rate of semileptonic decays such as $D \to \pi\ell\nu$ and $B \to \pi\ell\nu$ to a few percent, which corresponds to $\delta V_{\rm ub}^{\rm stat.} \sim 1-2\%$ [33]. However many consistency checks will be required to demonstrate that the estimated lattice precision has been achieved. Here we outline one possible method. From an unquenched LQCD calculation of f_D and a measurement of $D^+ \to \mu^+\nu$ at a charm factory (for example CLEO-C [35]) we obtain a precision direct measurement of $V_{\rm cd}$. Using this value of $V_{\rm cd}$, with an unquenched LQCD calculation of the rate and form factor shape of $D \to \pi\ell\nu$, we can make a direct test of the lattice with a measurement of $d\Gamma/dq^2(D \to \pi\ell\nu)$. If the lattice passes the above test, the second step is to compare the lattice prediction of the shape of $d\Gamma/dq^2(B \to \pi\ell\nu)$ to that of data at a B factory. If the shapes agree, the third step is to measure $\Gamma(B \to \pi\ell\nu)$ with data. Combining the measurement with the lattice prediction of $\Gamma(B \to \pi\ell\nu)$, we extract $V_{\rm ub}$. The theoretical error on $|V_{\rm ub}|$ may be as small as $1-2\%$. Table III shows the results of our simulation. To have a comparably small experimental error would require 10 ab^{-1}.

Uncertainty in V_{ub}

Inclusive methods will achieve $\delta V_{\rm ub} \sim 1-2\%$ from experiment and $\sim 5-10\%$ from theory, using the q^2 endpoint method with 2 ab^{-1} of data. If the lattice can reach the predicted accuracy of $1-2\%$, then exclusive measurements will provide the most precise determinations of $V_{\rm ub}$. Data samples on the order of 10 ab^{-1} will be required to attain a total experimental error of 1-2% on $V_{\rm ub}$ commensurate with the lattice error. However the

lattice must first be calibrated. Measurements of charm semileptonic decays can provide unique and crucial tests of the lattice predictions.

RARE DECAYS

Flavor-changing neutral currents are forbidden in the Standard Model (SM) at tree level but can occur via loop or box processes. Additional contributions can arise from New Physics processes such as new gauge bosons, charged Higgs bosons or supersymmetric particles. Rare B decays, occurring primarily through loops in the SM are also fertile searching ground for New Physics.

$B \to X_s\gamma$

Observation of the radiative penguin decay, $B \to X_s\gamma$, was the first direct evidence for an electroweak loop diagram. This decay is dominated by the magnetic penguin operator $O_{7\gamma}$, so the decay rate is proportional to the squares of the CKM matrix elements V_{ts} and the Wilson coefficient C_7. New physics processes yield additional contributions to C_7 and a new contribution C_8. Short distance calculations with next-to-leading order (NLO) QCD corrections have been carried out to 10% precision, $(3.3 \pm 0.3) \times 10^{-4}$[36]. Uncertainties in the renormalization scale accounts for 5% and the input parameters for roughly 8% of the theoretical errors. Comparing the above theoretical value with the total inclusive rate measurements from CLEO [37], limits on new physics beyond the SM have been set [38]. For example, the limit on the mass of a charged Higgs in the 2HDM model is greater than 250 GeV, as shown in Fig. 8 [38]. We expect the theoretical errors to be reduced to the 5% level with improvements in lattice QCD calculations of the scaling and better experimental determination of the input parameters.

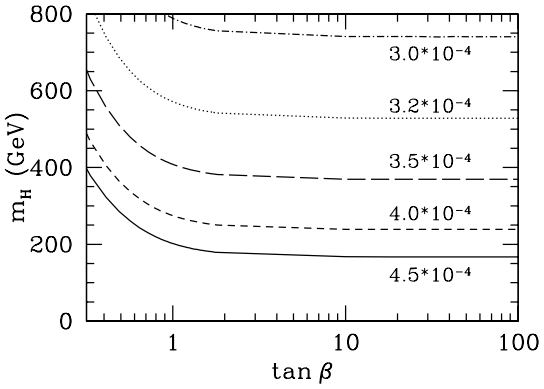

FIG. 8: Contour plot of limit on Charged Higgs mass as a function of tanβ in Type II 2HDM model. The allowed region is above the corresponding curves.

At higher luminosity B factories, systematic uncertainties will be the limiting factor in $B \to X_s\gamma$ as the statistical errors become negligible. The recent CLEO measurement of $B(B \to X_s\gamma) = (2.85 \pm 0.35 \pm 0.22) \times 10^{-4}$ has managed to reduce the systematic errors to 8% level[39]. The main backgrounds originate from $q\bar{q}$ continuum processes with either a high-energy photon from initial state radiation (ISR) or a π^0. The analysis combined three techniques to suppress continuum backgrounds: event shape analysis, reconstruction of the X_s system recoiling against the photon, and tagging of the other B with a high momentum lepton. The E_γ signal region was lowered to 2.0 GeV covering 94% of the spectrum, hence greatly reducing systematic errors from the modeling of the X_s mass distribution. However, the event shapes and X_s reconstruction efficiency are still dependent on the track multiplicity in $X_s \to K + n\pi$. This model dependency will make it difficult to reduce the systematic errors further with this technique at high luminosity B factories. Extrapolations of the CLEO measurement to 0.5 ab^{-1} and 10 ab^{-1} are shown in Table IV.

However, using the B tag sample, we can measure the inclusive rate for $B \to X_s\gamma$ from the E_γ distribution, without relying on the details of the X_s system. Precise measurement of the photon energy spectrum will also be useful in determining the parameters, m_b and P_f (Fermi motion of the b quark) which are used in non-perturbative calculations[40]. In 10 ab^{-1} of data, we expect inclusive rate measurements with a precision of 2-3% from systematic sources. With such results, correspondingly good constraints can be placed on non-SM physics, when the measured rate is compared to SM calculations having 5% uncertainty.

In addition to branching fractions measurements, *CP* asymmetries provide another test of the SM. While *CP* asymmetries are rather small in the SM, they may be a few percent in models beyond the SM. In the inclusive channel CLEO found a value $A_{CP}(B \to X_s\gamma) = (-0.079 \pm 0.108 \pm 0.022)$. We expect both statistical and systematic errors will be reduced to the 1-2 % level in 10 ab^{-1} of data.

$B \to K^*\gamma$ and $B \to \rho(\omega)\gamma$

At a 10^{36} B factory, we will be able to measure the $B \to K^*\gamma$ branching ratio accurately with high statistics. However, due to the large theoretical uncertainty in the $(K^*\gamma$ / $X_s\gamma)$ ratio, it is not possible to test the SM in exclusive decay rates. Conversely, we can test form factor models and Lattice QCD models for these decays in non-perturbative QCD regime. *CP* asymmetry in this mode is small ($< 1\%$) in the SM, but again new physics could enhance the asymmetry.

In a recent *BABAR* analysis[41] $B \to K^*\gamma$ was reconstructed in all 4 different $K\pi$ final states with a signal

yield of 237 events in 21 fb^{-1} of data. The branching ratio averaged over the four modes was $(4.11 \pm 0.34 \pm 0.20) \times 10^{-5}$, with a *CP* asymmetry of $A_{CP} = -0.044 \pm 0.076 \pm 0.012$. Extrapolating to 0.5(10) ab^{-1}, we have 6K(120K) events with a corresponding $\delta(A_{CP})$ of $0.02(< 0.01)$.

We also expect a signal in the CKM suppressed modes, $B \to \rho\gamma$ and $\omega\gamma$. With a ratio for $|V_{td}|^2/|V_{ts}|^2$ of order 1/20, we will have 300 and 6000 events in 0.5 and 10 ab^{-1}. Good K/π separation is crucial in suppressing the feed across from the larger $K^*\gamma$ decays. Direct *CP* asymmetry in the $\rho^+\gamma$ mode can be used to determine the CKM angle α[42]. The CP asymmetry and the $\rho\gamma/K^*\gamma$ ratio are also sensitive to MSSM SUSY models which predict substantial enhancement over the SM value[43].

$B \to X_s\ell\bar{\ell}$

The radiative decays $B \to X_s\ell^+\ell^-$ are smaller than $B \to X_s\gamma$ by about two orders of magnitude. Besides the magnetic penguin operator $O_{7\gamma}$, the semileptonic operators O_{9V} and O_{10A} contribute. The decay rates depend on the three Wilson coefficients $C_7^{eff}(m_b)$, $C_9^{eff}(m_b)$ and $C_{10}(m_b)$. For the inclusive modes the SM prediction is $Br(B \to X_S\ell^+\ell^-) = (6 \pm 1) \times 10^{-6}$. This Z/EM penguin decay is experimentally clean and also very sensitive to non-SM physics, because QCD corrections are smaller than in $B \to X_s\gamma$.

An inclusive analysis similar to the $X_s\gamma$ analysis can be carried out by reconstructing the recoiling X_s system against the lepton pair. Loss of efficiency for detecting two leptons instead of a single photon can be offset by relaxing continuum suppression cuts. With an estimated detection efficiency of 4%, we expect about 300(350) events in the $X_s\mu^+\mu^-(X_se^+e^-)$ decay mode for 0.5 ab^{-1} of data,

The *CP* asymmetry in the SM for $B \to X_s\ell^+\ell^-$ is very small, $O(10^{-3})$. In certain unitarity-violating models such as the extra isosinglet quark model[44], the asymmetry can be enhanced by up to 2%, which is the sensitivity level expected in 10 ab^{-1}.

The exclusive decay $K^*\mu^+\mu^-$ has recently been identified as a good place to look for non-SM physics effects. The forward/backward asymmetry between the K^* and μ^+ directions in the di-muon center-of-mass frame has a zero-crossing at a certain q^2 value, where q is the mass of the di-muon system. In the SM, this zero-crossing point is well predicted[45]; any deviation would indicate evidence of new physics [46]. With a branching ratio of 1.5×10^{-6} and detection efficiency of 8%, we expect to observe 120(2400) events in 0.5(10) ab^{-1}. The electron mode has slightly higher efficiency and will add another 150(3000) events to the observed sample.

$B \to X_s\nu\bar{\nu}$

This Z-penguin decay process $B \to X_s\nu\bar{\nu}$ is theoretically clean since there are no contributions from the EM penguin diagrams. At the expected rate of 4×10^{-5}, it can provide a stringent test of new physics beyond the SM, for example SUSY[47]. With two missing neutrinos in the detector, however, it is very challenging experimentally to make a precise measurement, or even to observe it. The current limit, 7.7×10^{-4} (90% CL), is from ALEPH[48] where they utilized the large missing energy in this mode to suppress background from other Z decays. The largest source of background is $B \to \tau\bar{\nu}$ which is indistinguishable from the signal.

At the $\Upsilon(4S)$, a similar analysis can be carried out using fully tagged B's. In a sample of 2 million fully reconstructed B tags for 0.5 ab^{-1}, there are roughly 80 $X_s\nu\bar{\nu}$ events. We require a kaon and n pions (where n=0,1,2,3) and large missing energy in the rest of the event. Combining the q^2 distribution of the $Kn\pi$ system and the direction of the missing momentum vector can be used to suppress backgrounds from other B decay modes. The particle identification system (DIRC) in *BABAR* already provides very good K/π separation which is essential for this analysis, since the main source of background $B \to \tau\bar{\nu}$ produces n pions in hadronic τ decay modes. We expect a detection efficiency of roughly 10% with the assumption that the X_s mass and n pion multiplicity distributions are similar to the ones in $B \to X_s\gamma$. Due to the requirement of having to use B tags, the number of signal events is not large, 8(160) in 0.5(10) ab^{-1}. In the larger data set, it might be possible to test MSSM contributions which could be as much as ±35%[47].

Analysis of the exclusive decays $B \to K^{(*)}\nu\bar{\nu}$ is similar to the inclusive case, with an additional requirement that there are no other particles in the event. The momentum distribution of the $K^{(*)}$ can also be used to background suppression, but it does not appear to be a very effective variable. The estimated detection efficiency of 15% will depend on the level of beam and physics backgrounds in the Super*BABAR* detector.

$B^- \to \ell^-\bar{\nu}$

These tree-level electroweak processes are helicity-suppressed in the SM. They are therefore theoretically clean and provide direct sensitivity to the product $V_{\rm ub}f_B$:

$$\mathcal{B}(B^- \to \ell^-\bar{\nu}) = \frac{G_F^2|V_{\rm ub}|^2}{8\pi} f_B^2 \tau_B m_B m_\ell^2 \left(1 - \frac{m_\ell^2}{m_B^2}\right)^2$$

The $B \to \mu\nu$ and $\tau\nu$ modes are particularly interesting, since the branching ratios ($\sim 2 \times 10^{-7}$ and $\sim 5 \times 10^{-5}$, respectively) are likely to be just within the reach of existing B factories, while the extreme helicity suppression

of the $e\nu$ mode ($\mathcal{B} \sim 5 \times 10^{-12}$) leaves it completely inaccessible. Sensitivity to non-SM physics may be obtained by either a comparison of these modes with the SM rate prediction, or by comparison of the relative rates. The former assumes f_B to be independently understood and sufficiently well known from a theoretical basis, (precise measurements of f_D and f_{D_s} from existing B factories, will already exist as input to lattice calculations), while the latter, eliminates this prerequisite. The exchange of a charged Higgs for example, will be enhanced in the $\tau\nu$ mode relative to $\mu\nu$ due to the lepton mass, leading to a deviation from the SM prediction.

In the case of $\mu\nu$, the muon is mono-energetic in the B meson rest frame, leading to a relatively clean signature for this mode at an e^+e^- collider at the $\Upsilon(4S)$. In practice, the muon is observed to recoil against a second B which can be inclusively reconstructed using a simple four-vector sum of *everything else* in the event. The overall reconstruction efficiency is expected to be on the order of $5 - 15\%$.

In contrast to the $\mu\nu$ channel, the additional missing neutrino(s) from the τ decay in $B \to \tau\nu$ means that constraint on the lepton momentum cannot be fully exploited. In order to measure this mode it is necessary to fully reconstruct the recoiling B^+ in some hadronic or semileptonic decay mode, for example $B^+ \to D^0\pi^+$, and then identify the $B \to \tau\nu$ signal with the remaining reconstructed objects in the event. Monte Carlo simulation suggests an important correlation between the purity required for the B tag reconstruction and the τ decay mode identified in the recoil. Figure 9 for example demonstrates how a lower-purity (higher efficiency) hadronic B tag can be cleanly discriminated when it is tagging a generic τ decay in contrast to tagging another hadronic B decay.

It is estimated that between 45% and 85% of the available τ branching ratio can be used, by adjusting the tag purity in this manner. The ability to relax the B tag purity (in a manner dependent on the complexity of the recoil τ) will result in an improved effective tagging efficiency. The expected efficiency for fully reconstructing the recoil B is likely to average about 0.2%, while on the $\tau\nu$ side it will be $\sim 30\%$. This leads to an overall yield of 17 (8) events in 0.5 ab^{-1} for $\tau\nu(\mu\nu)$. It is important to note that in all modes with missing neutrinos, and for $B \to \tau\nu$ in particular, beam backgrounds may be a limiting factor in whether or not the measurement will be possible.

Using these estimated efficiencies, existing B factory experiments should have sensitivity to both the $\tau\nu$ and $\mu\nu$ modes, however measuring their relative branching ratios to better than 20% precision will require more than 0.5 ab^{-1} of data. With a data sample of 10 $ab^{-}1$ the statistical error on $\mathcal{B}(B \to \tau\nu)$ and $\mathcal{B}(B \to \mu\nu)$ would be reduced to $\sim 5\%$ and $\sim 8\%$, respectively. The theoretical uncertainties in $f_B|V_{ub}|$ and other systematic errors

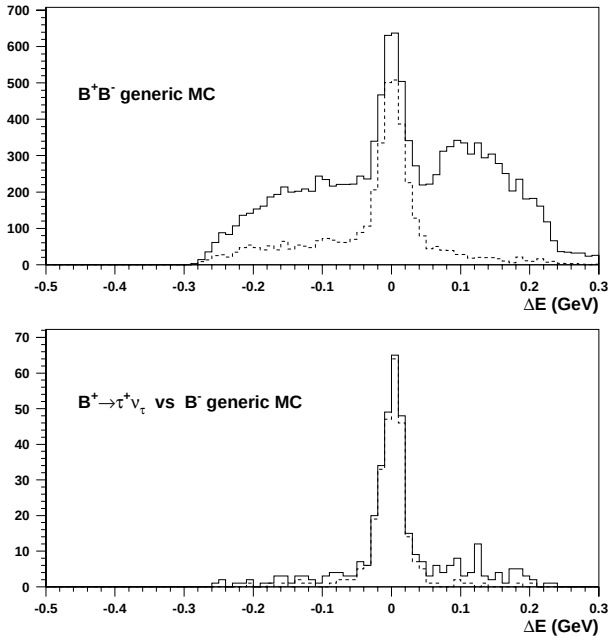

FIG. 9: ΔE distributions (solid) for reconstructed $B_{\rm tag}$: ($B^+_{\rm tag} \to D^{*0}\pi^+$, $D^{0*} \to \gamma D^0$, $D^0 \to K^+\pi^-\pi^+\pi^-$) for generic B^+B^- Monte Carlo events (top) and for $B^+ \to \tau^+\nu$ vs a generically decaying B^- (bottom). The lower (dashed) histograms within each figure show the subset of events in which the reconstruction has correctly identified the tag mode.

should contribute 2 - 4% to each, implying absolute rate comparisons with SM predictions remaining close to the 5% (8%) level, respectively. A comparison of the relative rates would have an error of $\sim 9\%$, as theoretical and other systematic errors largely cancel. Owing to the relatively limited kinematic constraints available on these modes, it is unlikely that either of these channels will ever be accessible at hadron machines.

$$B^0 \to \ell^+\ell^-$$

In the SM these modes are mediated by box or loop diagrams and have branching ratios $B(B^0 \to e^+e^-) \sim 10^{-15}$, $B(B^0 \to \mu^+\mu^-) \sim 10^{-10}$, and $B(B^0 \to \tau^+\tau^-) \sim 10^{-8}$. In addition, lepton flavor-violating decays (i.e. $B^0 \to e^\pm\mu^\mp$) are strictly forbidden in the Standard Model. Since all of these decay modes are highly suppressed and many extensions of the SM significantly enhance their rates, they provide an excellent way to search for new physics. For example, the decay could proceed through new gauge bosons that induce flavor changing neutral currents (FCNC) or leptoquarks, which violate

lepton flavor. New physics mechanisms which have mass dependent couplings may be more readily seen in B decays than in lighter meson decays, and may favor heavier leptons in the final state.

For $\ell = e, \mu$, the two leptons can be used to obtain the B^0 four-vector, leading to a clean experimental signature at both hadronic and e^+e^- machines. Consequently, a 10^{36} B Factory will not be competitive in these modes. However, in the case of $B^0 \to \tau^+\tau^-$ or $B^0 \to \tau^+\ell^-$ ($\ell = e, \mu$) the neutrino(s) produced by the τ decay effectively remove the invariant mass constraint on the signal B, making these modes extremely difficult at hadron machines. At an $\Upsilon(4S)$ machine, the experimental signature would be two τ *jets* consisting of leptons or pions, with significant missing energy, recoiling against a fully reconstructed B^0. The requirement of reconstructing the recoil B would limit the efficiency to the level of 0.2%. With an integrated luminosity of 10 ab^{-1}, the branching fraction sensitivities for the various $B^0 \to \ell^+\ell^-$ modes are as follows:

- $ee, \mu\mu,$ or $e\mu$: $< 5 \times 10^{-9}$
- $e\tau$, $\mu\tau$: $< 5 \times 10^{-7}$
- $\tau\tau$: $\sim 2 \times 10^{-6}$.

These limits may be interpreted in the context of specific new physics scenarios. Figures 10 and 11 show the 10 ab^{-1} sensitivities for a leptoquark and SUSY model without Rparity. The mass limits reach beyond 10 TeV in both cases, for coupling strengths at the electroweak scale.

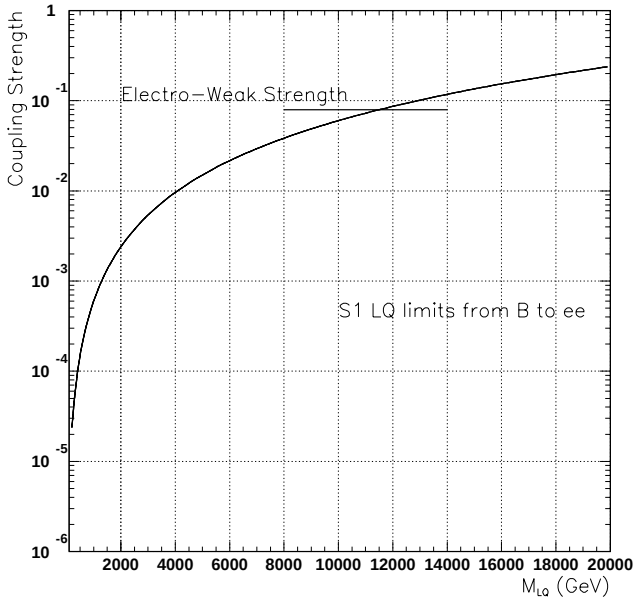

Figure 1: The 90% CL limits on coupling versus leptoquark mass.

FIG. 10: 90% confidence level limits on coupling *vs.* leptoquark mass.

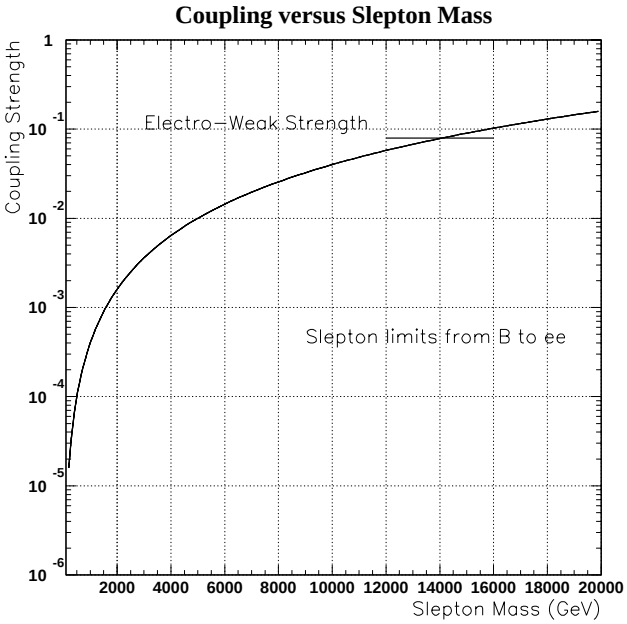

Figure 2: The 90% CL limits on coupling versus slepton mass.

FIG. 11: 90% confidence level limits on coupling *vs.* R-parity-violating slepton mass.

$$B^0 \to \gamma\gamma$$

This annihilation penguin, or vertical penguin, process is suppressed in the SM by $(f_B/m_B)^2$. The SM branching ratio is around 10^{-8} [49], while non-SM contributions (2HDM, Z^0 FCNC) could enhance it by as much as $O(10^2)$ [50]. The current branching ratio limit for $B^0 \to \gamma\gamma$ is $< 1.7 \times 10^{-6}$[51] from *BABAR*. The main sources of background in searching for this decay mode are high momentum π^0's from the $q\overline{q}$ continuum and π^0's and photons from other rare B decays such as $B \to \pi^0\pi$, $B \to \pi^0 K$ and $B \to X_s(X_d)\gamma$. The detection efficiency in *BABAR* analysis after continuum suppression and anti-π^0 cuts is around 8%. Extrapolation to 0.5 and 10 ab^{-1}, assuming that the same efficiency to background ratio can be maintained, give us 0.4 and 8 events, respectively.

Comparison of hadronic and e^+e^- rare B decay samples

Table IV is a comparison of the capabilities of hadronic and e^+e^- colliders in accumulating samples of rare B decays. Experiments at hadronic machines will have advantages in decay modes with all charged particle final states which form detached vertices. One good example is the decay $B^- \to K^-\mu^+\mu^-$, where the 3-prong decay vertex and good identification of the muon pair will provide efficient triggering and excellent background suppression. However, in decay modes that involve neutral particles such as π^0, γ, and ν, e^+e^- factory experiments are clearly favored. Especially, with a large number of Tagged B

events at high luminosity machines, reconstruction of final states with 2 or 3 neutrinos will be possible. One notes that of all the decay modes listed in Table IV, only 1 event candidate for $B \to K^*\gamma$ has ever been observed at hadronic experiments (by CDF). In summary, hadronic and e^+e^- experiments play complementary roles in rare B decay studies. If non-SM physics effects are observed in B decays, study of different final states will tell us much about the detailed nature of new physics.

OTHER PHYSICS

τ physics

An electron positron collider with high luminosity is an excellent tool for τ physics; 10 ab^{-1} corresponds to a sample of 10^{10} τ^+ τ^- events. In addition to the more conventional τ physics possible, this large sample of τ's will permit searches for lepton flavor violating decays. As the heaviest lepton, τ decays are a promising probe of new physics related to mass generation[52].

In the Standard Model, processes like $\tau \to \mu\gamma$ are suppressed by $\delta m_\nu^2/M_W^2$, and observation of lepton flavor violation is a clear signature of new physics. Many supersymmetric models [53] predict sizeable contributions to the $\tau \to \mu\gamma$ decay given by the diagrams:

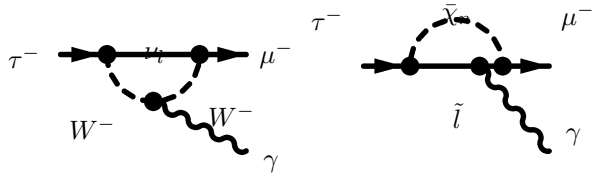

(2)

In these graphs the internal lines are dressed with a charged slepton ($\tilde{l}$) and a neutralino ($\bar{\chi}_n$) or by a sneutrino ($\tilde{\nu}$) and a chargino ($\bar{\chi}_c$). Depending on the supersymmetric parameter these models predict $\mathcal{B}(\tau \to \mu\gamma)$ ranging from 10^{-7} to 10^{-9} which is experimentally reachable at a very high luminosity e^+e^- collider running at the $\Upsilon(4S)$.

At present the 90% confidence level upper limit on the lepton flavor violating τ decays are: $\mathcal{B}(\tau \to \mu\gamma) < 1.1 \times 10^{-6}$ and $\mathcal{B}(\tau \to e\gamma) < 2.7 \times 10^{-6}$ both set by CLEO using 12.6×10^6 τ^+ τ^- pairs.

A recent study evaluated the branching ratio reach for $\tau \to l\gamma$, using τ^+ τ^- events in which one τ decays to hadrons, $\tau \to n\pi\nu_\tau$, and the other is used to search for the lepton flavor violating decay. The only undetected particle is a neutrino whose four momentum can be reconstructed relying on momentum conservation and provides an important background suppression. In particular the decay $\tau \to 3\pi$ $(\pi^0)\nu_\tau$ has the advantage of a clean topological signature with three tracks in a narrow jet, a small contamination from QED processes, and the possibility to exploit the excellent vertex resolution to discriminate against light quark continuum events. Backgrounds were evaluated using a full GEANT simulation of the *BABAR* detector and an 8 fb^{-1} sample of simulated $q\overline{q}$ and τ^+ τ^- decays. A complete analysis was done using a realistic event selection with reduced the $q\overline{q}$ contamination to 2%. To further discriminate against $q\overline{q}$ and ordinary τ decays, the missing mass and energy and the reconstructed τ mass and energy were used. Given an estimated background level of 20 ± 20 events in 10 ab^{-1}, and an efficiency of 30% for $\tau \to 3\pi$ $(\pi^0)\nu_\tau$, makes a branching ratio for $\tau \to l\gamma$ of 10^{-8} experimentally possible. This level of sensitivity is unlikely to be possible at any other experimental facility.

Production of charm via ISR

The study of meson and baryon production by initial state radiation at a very high luminosity asymmetric B Factory appears extremely promising.

Initial State Radiation (ISR) events $e^+e^- \to \gamma(e^+e^- \to X)$, where $X = \rho, \phi, J/\psi, \psi(2S)$, produced at the $\Upsilon(4S)$ energy have been directly observed by the *BABAR* experiment [54]. The potential of physics using ISR events at B Factory experiments has been previously noted [55]. For a SuperPEP-II machine with a peak luminosity of 10^{36} cm^{-2}s^{-1}, ISR events provide greater physics potential. The ISR data can be used to study R, form factors, model independent measurement of the D_s, D^+ mesons and charmed baryons, as well as to study charmonia and search for glueballs and hybrids, and it provides access to e^+e^- collisions down to very low CM energies.

In the CM system of the electron-positron, an ISR event can emit a hard photon, with energy E_γ, resulting in a subsequent e^+e^- annihilation at a reduced CM energy $\sqrt{s'}$, which is related to the CM energy, $\sqrt{s}$: $s' = \sqrt{s}(\sqrt{s} - 2E_\gamma)$. Given E_γ, the CM energy of the e^+e^- annihilation can be directly determined. The differential production cross section for a specific process is

$$\frac{d\sigma}{dk} = f(s,k) \cdot \sigma(s)$$

where $k = 2E_\gamma/\sqrt{s}$, $f(s,k)$ is a sampling function, and

		Hadron Collider Experiments			e^+e^- B Factories	
Decay Mode	Branching Fractions	**CDF D0** (2 fb^{-1})	**BTeV LHCb** (10^7 s)	**ATLAS CMS** (1 Year)	***BABAR*** **BELLE** (0.5 ab^{-1})	**10^{36}** (10 ab^{-1})
$B \to X_s\gamma$	$(3.3 \pm 0.3) \times 10^{-4}$				11K 1.7K (B Tagged)	220K 34K (B Tagged)
$B \to K^*\gamma$	5×10^{-5}	170	25K		6K	120K
$B \to \rho(\omega)\gamma$	2×10^{-6}				300	6K
$B \to X_s\mu^+\mu^-$	$(6.0 \pm 1.5) \times 10^{-6}$		3.6K		300	6K
$B \to X_s e^+e^-$					350	7K
$B \to K^*\mu^+\mu^-$	$(2 \pm 1) \times 10^{-6}$	60-150	2.2K/4.5K	665/4.2K	120	2.4K
$B \to K^* e^+e^-$					150	3K
$B \to X_s\nu\overline{\nu}$	$(4.1 \pm 0.9) \times 10^{-5}$				8	160
$B \to K^*\nu\overline{\nu}$	5×10^{-6}				1.5	30
$B^0_d \to \tau^+\tau^-$	10^{-7}					
$B^0_s \to \mu^+\mu^-$	10^{-9}	5/1.5-6	5/11	9/7		
$B^0_d \to \mu^+\mu^-$	8×10^{-11}	0/0	1/2	0.7/20		
$B \to \tau\nu$	5×10^{-5}				17	350
$B \to \mu\nu$	1.6×10^{-7}				8	150
$B^0 \to \gamma\gamma$	10^{-8}				0.4	8

TABLE IV: Comparison of the number of reconstructed rare B decays in hadronic and e^+e^- experiments

Production interaction $e^+e^- \to \gamma(e^+e^- \to X)$	$\sqrt{s'}$ (GeV)	Fraction of sampling funct.	Cross-section	Produced events (10^6) per ab^{-1} of data
$D_s^+D_s^-$ - $D_s^+\overline{D}K$	3.94 - 4.33	0.00167	1 nb	1.7
$D\overline{D}/D^*\overline{D}/D^*\overline{D^*}$	4.0 - 4.6	0.00273	6 nb	16
$\Lambda_c^+\Lambda_c^-$ - $\Lambda_c^+\overline{D}\overline{p}$	4.57 - 5.09	0.00284	0.4 nb	1.1
J/ψ	3.097		36 pb	36
ψ(2S)	3.686		14 pb	14
Υ(1S)	9.460		19 pb	19
Υ(2S)	10.023		15 pb	15
Υ(3S)	10.355		31 pb	31

TABLE V: Estimate of ISR Charm Rates

$\sigma(s)$ is the nominal production cross section at the CM energy $\sqrt{s'}$ for this process [56].

For charmed hadrons the energy ranges for $\sqrt{s'}$ near the production thresholds, as listed in Table V, are chosen such that a specific charmed hadron produced in pairs can be identified unambiguously by a fully reconstructed charm decay (for the D_s and the Λ_c^+), a method referred to as a single tag, or by using the Recoil Charge Method developed by BES [57] that identifies the D^+ statistically. The fractional sampling functions indicate an effective e^+e^- luminosity of $\sim 2 \times 10^{33}$ cm^{-2}s^{-1} for ISR events produced around the charm threshold region, as listed in Table V. The nominal production cross sections are taken from Ref. [58] for charmed mesons, and an earlier Mark II measurement of the Λ_c^+ production rate is used [59], assuming a linearly falling cross section for the Λ_c^+ in the energy range listed in Table tab:isr1. Estimates for charmonia and bottomonia are those of Ref. [55], scaled to the benchmark luminosities, 0.5 ab^{-1} and 10 ab^{-1}, respectively.

The ISR charm events are selected by detecting a high energy photon ($\geq$4 GeV in the CM) or the presence of a large missing momentum ($\geq$ 4 GeV, CM) along the beam direction, that is, opposite a fully reconstructed charm hadron.

Estimates for the number of events detected in a variety of decay modes are shown in Table VI. Typical *BABAR* detector efficiencies were used. For a SuperPEP-II experiment with an integrated luminosity of 10 ab^{-1}, the statistical error limits are $\leq$0.3 - 2.0 % for hadronic branching fractions of charmed hadrons, 3% or less for leptonic charm decays; all determinations are model independent. The ISR data are, of course, collected at all $\sqrt{s'}$ below the $\Upsilon(4S)$ energy.

SuperPEP-II: A 10^{36} Collider

Decays	Produced events ($\times 10^6$) in 10 ab^{-1}	BR x detection efficiency (%)	Events reconstructed (10^3)	Relative statistical error(%)
D_s^+ branching fraction	~ 17	0.026	4.4	1.5
D_s^+ leptonic decays	~ 17	0.039	.6	1.2
D^+ leptonic decays	~ 53 (1/3 per D pair)	0.0019	1.0	3.2
$D^+ \to K^-\pi^+\pi^+$	~ 53 (1/3 per D pair)	0.25	132	0.3
Λ_c^+ branching fraction	~ 11	0.025	2.75	1.9
J/ψ	360	0.3	1,080	0.1
$\psi(2S)$ leptonic width	140	0.067	93.8	0.3

TABLE VI: Estimate of ISR signal events for 10 ab^{-1}

The existing B Factories PEP-II and KEK-B have reached luminosities of $(3-4)\times 10^{33}$ cm^{-2}s^{-1} and delivered integrated luminosity at rates in excess of 4 fb^{-1} per month [60], [61]. The recent turn-on of these two B Factories has shown that modern accelerator physics, design, and engineering can produce colliders that rapidly reach their design luminosities and deliver integrated luminosities capable of frontier particle physics discoveries. With ongoing upgrade programs PEP-II and KEK-B should reach luminosities of over 10^{34}cm^{-2}s^{-1} in a few years and with more aggressive improvements may reach luminosities of order 10^{35}cm^{-2}s^{-1} by the end of the decade. However, due to particle physics requirements, the next generation B Factory may require significantly more luminosity. Initial parameters of a very high luminosity e^+e^- B Factory or Super B Factory (SBF) are being developed incorporating several new ideas from the successful operation of the present generation e^+e^- accelerators [62], [63].

A luminosity approaching 10^{36}cm^{-2}s^{-1} appears possible. Furthermore, the ratio of average to peak luminosity may be increased by 30% due to continuous injection. The operation of this accelerator will be qualitatively different from present e^+e^- colliders due to this continuous injection. A detailed discussion of the effect of backgrounds will be presented in the detector section.

DESIGN CONSIDERATIONS

The next generation e^+e^- B Factory will likely operate at the $\Upsilon(4S)$ with a center-of-mass energy of 10.58 GeV and with the same energy asymmetry as present. For the study here the PEP-II tunnel geometry was used as well as the PEP-II beam energies of 9.0 and 3.1 GeV. The choice of energy asymmetry is, at this time, an open question as a larger energy asymmetry makes the beam separation at the interaction region easier but it makes the RF costs larger. To increase the luminosity about two orders of magnitude the beam currents must be raised an order of magnitude and the beam cross sectional area reduced an order of magnitude while keeping the beam-beam tune shifts under control. The parameters below are self-consistent but further overall optimization can be made.

LUMINOSITY AND INTEGRATED LUMINOSITY

The luminosity can be calculated in several ways [64]. A convenient scaling formula for the luminosity $\mathcal{L}$ is shown below. E is the beam energy (GeV), r the y/x size aspect ratio, xy the vertical tune shift limit, I the beam current (A), and β_y the vertical β function at the IP. Note that the tune shift xy and the current I are not independent. The number of bunches is also a variable.

$$\mathcal{L} = 2.17\times 10^{34}(1+r)\xi_y\frac{EI}{\beta_y}[\mathrm{cm}^{-2}\mathrm{s}^{-1}]$$

In order to achieve a luminosity near 10^{36}cm^{-2}s^{-1} for the Low Energy Ring (LER) at 3.1 GeV, the following approximate parameter values are needed: $\beta_{x,y} = 0.33$ cm, $\xi_y = 0.14$, $r = 1.0$ and $I = 20$ A. For the High Energy Ring (HER) at 9 GeV, $\beta_{x,y} = 0.33$ cm, $xi_y = 0.14$, $r = 1.0$ and $I = 6.5$ A.

The integrated luminosity will also increase by a separate factor of about 1.35, as this collider will need continuous injection making the average to peak luminosity about 0.95, as opposed to the present colliders which have ratios of about 0.7.

OVERALL DESIGN PARAMETERS AND CONSTRAINTS

The overall parameters discussed above were used to make an accelerator design. The detailed parameters are shown in Table VII. The design choices and constraints are many. The two beam energies force two

separate rings. There is one collision point. The circumferences are equal due to beam-beam interaction reasons. Round beams will be used to increase the beam-beam tune shifts. However, flat beams have traditionally worked well but reduces the peak luminosity by a third given the same currents. Several RF frequencies are possible but 476 MHz was selected, as that is the present PEP-II frequency. The number of RF cavities must be increased with the beam current. Every RF bucket has a bunch. The interaction region is similar to that of PEP-II but must be longitudinally shortened to keep the peak betas in the interaction region quadrupoles as low as possible. Since the bunches are significantly shorter, a crossing angle can be used at the collision point to help separate the beams. The beam lifetimes will be low forcing injection to be continuous. Continuous injection will also allow the beam-beam tune shift limits to be increased. The HER will store positrons to reduce the effects of the electron cloud instability. The very high electron current in the LER will likely remove all collected ions. If not, clearing electrodes may have to be installed. The vacuum chambers may be a continuous extrusion, welded together to minimize impedance issues and reduce the number of fragile vacuum elements such as bellows. The present magnetic lattice for the LER is adequate but the magnet lattice for the HER ring must be modified for a lower momentum compaction factor to reduce the bunch length. This can be accomplished by increasing the phase advance per cell, combined function magnets, or additional quadrupoles.

BEAM-BEAM TUNE SHIFTS

The observed beam-beam tune shifts in PEP-II are approaching 0.07 [61]. The expected tune shifts in this new accelerator should be larger for two reasons. Theoretical and experimental evidence indicates that round beam operation of the collision point will increase the tune shifts by about a factor of two. However, there may be increased backgrounds from round beam operation but significantly more backgrounds are expected from other sources as well. Furthermore, it has been observed in PEP-II during routine running that by adjusting the tunes the luminosity can be increased significantly ($\sim 10\%$) at the expense of the beam lifetime [65]. (This beam lifetime will be called the beam-beam lifetime.) Higher luminosity for the same current means higher tune shifts. It is believed that this new accelerator can take advantage of continuous injection to push the tune shifts to significantly higher values and consequently the beam-beam lifetimes to significantly lower values. The beam-beam lifetime in present colliders is about 100 minutes. The assumption used in this note is that the tune shifts can be increased from 0.07 to 0.14 by reducing the beam-beam lifetime from 100 minutes to 10 minutes and by adopting round beams at the collision point.

INTERACTION REGION

The interaction region will likely have a similar geometry to that of PEP-II [66]. The cone angle separating the accelerator and detector components can be the same at about 300 mrad. The focusing quadrupoles must be as close to the interaction point (IP) as possible to reduce the peak beta functions in those quadrupoles. The LER quadrupoles for this accelerator can be moved significantly closer to the IP than in PEP-II using superconducting Q1 and Q2 magnets with stronger gradients. A good choice for these magnets are those used in the HERA upgrade[67]. The HER quadrupoles can also be moved closer because the LER quadrupoles have been moved. A crossing angle of about ± 1.5 mrad is used to help separate the beams at the first parasitic beam-beam crossing. The beams are horizontally separated by about 12 σ_x at the first parasitic crossing. Possible configurations for the LER and HER interaction regions are shown in Figure 12.

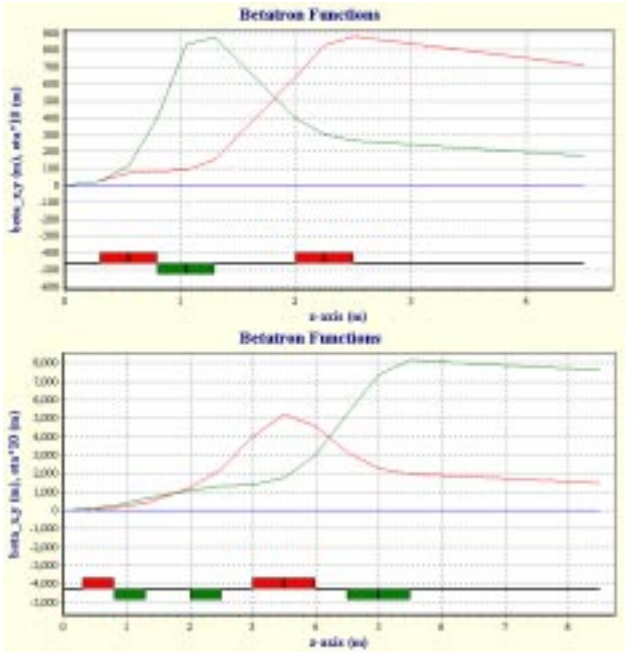

FIG. 12: Possible interaction region configuration for the LER (top) and HER (bottom) of a SBF.The β function is shown as a function of distance from the IP for the horizontal (red) and vertical (green) dimensions.

Parameter	High Energy Ring (HER)	Low Energy Ring (LER)
Beam energy (GeV)	9.0	3.1
Beam particle	e^+	e^-
Center of mass energy (GeV)	10.58	10.58
Circumference (m)	2200	2200
RF Frequency (MHz)	476	476
RF Voltage (MV)	50	30
Synch. Rad. Power (MW)	23	12
Number of bunches	3492	3492
Total beam current (A)	6.6	19.2
$\beta^*_{y/x}$ (cm)	0.32/0.32	0.32/0.32
Emittance (y/x) (nm)	22/22	22/22
Momentum Compaction	0.001	0.0013
Bunch length (mm)	3.5	3.5
Approx. AC power (MW)	50	27
Beam lifetime (min)	5	5
Injection particles per pulse	7.3×10^{10}	5.3×10^{10}
Continuous injection rate (Hz)	20	80
Beam-Beam tune shifts	0.14	0.14
Transverse beam size (μm)	8.4	8.4
Luminosity ($\mathrm{cm}^{-2}\mathrm{s}^{-1}$)	10^{36}	10^{36}

TABLE VII: 10^{36} Collider parameters based at the PEP-II tunnel

RF SYSTEM AND BEAM POWER

The RF system design can be similar to that of KEK-B or PEP-II but with an order of magnitude larger scale. The basic parameters are shown in Table VIII. The longitudinal beam dynamics will be difficult with the large beam currents. To keep the beams stable, it is likely that the solutions used for KEK-B (storage cavities) and for PEP-II (strong bunch-by-bunch feedbacks) will both be needed.

RF Parameter	LER	HER
RF frequency (MHz)	476	476
Number of klystrons	20	30
Number of cavities	40	70
RF voltage (MV)	30	50
Beam current (A)	19.2	6.6
Synch. Radiation Power (MW)	12	23
Bunch length (mm)	3.5	3.5

TABLE VIII: RF and beam power parameters for a new Super B Factory

VACUUM SYSTEM

The HER vacuum system must dissipate over 16 kW/m of synchrotron radiation power. The chambers will likely be made with an antechamber with a continuous built-in photon stop. A concept of the chamber is shown in Figure 13. The design of the bellow (expansion) modules will be very difficult for these high currents and short bunch lengths. Instead, the plan is to use a concept investigated for the PEP-II rings but not implemented. The vacuum system would be a continuous extrusion welded together with no bellows but with rigid supports to constrain thermal stresses [68]. A similar technique is used to build very long train welded railroad tracks. Moreover, the beam impedance will be better without bellows. The stainless steel chambers in the straight sections will need to be changed to a lower resistance material to reduce the resistive wall effect for the LER.

BEAM LIFETIME

The beam lifetime has several components. The five main contributors are discussed here. A summary is shown in Table IX giving a total beam lifetime of about 4 to 5 minutes for each beam, hence the need for continuous injection.

- Luminosity lifetime comes from particle losses from collisions. The loss rate is given by

$$\frac{dN}{dt}(t) = -\sigma \mathcal{L} dt$$

where N is the total number of particle in the beam. σ is the cross section for a scattered particle to leave

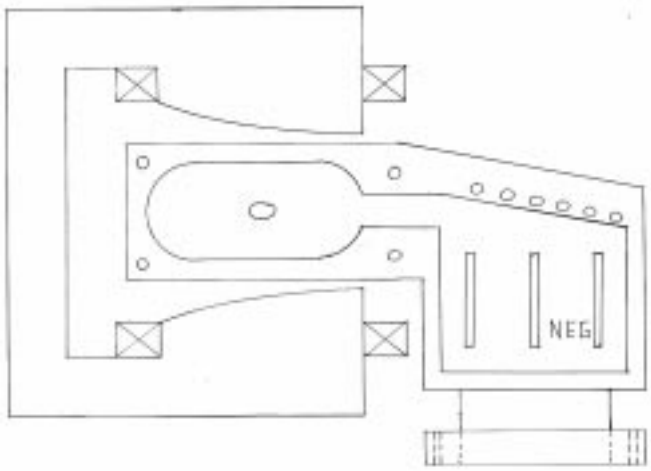

FIG. 13: Possible magnet and vacuum chamber configuration for the HER of a SBF.

the accelerator aperture, is about $3 \times 10^{-25}\text{cm}^{-2}$. At $\mathcal{L} = 10^{36}$, $dN/dt = 3 \times 10^{11}$ per second.

- The vacuum lifetime comes from beam-gas scattering. The vacuum pressure will likely be somewhat worse than PEP-II as there is more synchrotron radiation. Vacuum lifetimes one-third those of PEP-II are used.

- The Touschek lifetime comes from intra-bunch particle scattering. The approximate Touschek lifetimes in PEP-II are 3 hours for the LER and 30 hours for the HER. The lifetime for this collider can be scaled from these values. For this accelerator the bunch charges are higher than for PEP-II reducing the lifetime about a factor of two. The transverse sizes are larger than PEP-II due to round beams, thus, increasing the lifetime about a factor of two. However, the longitudinal size is three times smaller which will reduce the Touschek lifetime by a factor of three. Overall change is about a factor of three reduction.

- The beam lifetime from the beam-beam interaction will be reduced to about 10 minutes to maximize the beam-beam tune shifts.

- The beta functions in the interaction region quadrupoles are larger than those in PEP-II and will likely lead to reduced beam lifetime from a reduced dynamic aperture as determined from chromatic sextupole corrections. A lifetime from this effect is hard to predict but 20 minutes is used.

Lifetime Effect	HER	LER
Luminosity lifetime (min)	15	58
Vacuum lifetime (min)	100	30
Touschek lifetime (min)	600	60
Beam-beam tune shift lifetime (min)	10	10
Dynamic aperture lifetime (min)	20	20
Overall beam lifetime (min)	4.4	4.6

TABLE IX: Contributions to the beam lifetime

INJECTION

Injection must be a continuous process because the beam lifetimes are short. Taking the SLAC site, the beams would come from the damping ring and linac complex. The parameters for this system are shown in Table X. The SLAC system was built to provide about 1×10^{11} electrons per pulse at 120 Hz and about half that rate for positrons. The damping ring cavity RF frequency will be changed from 714 MHz to 476 MHz. In the damping rings, the particle bunches will be distributed uniformly over about half the circumference (35 m) in about 30 bunches. The other half of the ring circumference is used by the injection and extraction kicker rise times. The linac can operate at 120 Hz. The electron injection rate would likely be 80 Hz, the positron injection rate 20 Hz, and the remaining 20 Hz used for positron production. Injection losses can cause detector problems. However, the damped injected beam will have transverse emittances smaller than the stored beam emittances. Also, the linac bunch length and energy spread match well those of the stored bunches. Thus, the injection process should be relatively clean. However, as some injection collimation will likely be needed, the injection efficiencies were taken to be 75%.

Parameter	HER	LER
Number of beam particles	3.0×10^{14}	8.8×10^{14}
Particle type	e^+	e^-
Injection energy (GeV)	9.0	3.1
Beam lifetime (min)	4.4	4.6
Ring particles lost per second	1.1×10^{12}	3.2×10^{12}
Injection rate (Hz)	20	80
Injection efficiency	0.75	0.75
Injected particles per pulse	7.3×10^{10}	5.3×10^{10}
Bunches injected per pulse	30	30
Injected particles per bunch	1.8×10^{9}	1.3×10^{9}
DR RF frequency (MHz)	476	476

TABLE X: Injection parameters

APPROXIMATE COST

The cost of a future Super B Factory can be approximated using the original costs for PEP-II construction escalated for inflation with the addition of the special costs of new items (for example RF stations) and reduced by items that need little change (injection system). The biggest cost driver will be the RF system as many more stations are needed. A summary of the approximate costs is shown in Table XI.

WBS item	PEP-II Actual (M$)	Proposed SBF (M$)
HER Ring	55.0	35
LER Ring	48.4	30
Interaction Region	7.3	7
Injector	16.6	1
Controls	6.7	2
Utilities	7.4	5
Safety and Protection	1.8	1
Management	7.3	9
Machine RF (add'tnl 42 stations)	22.9	110
Indirects	3.4	35
Contingency	-	70
Sub-total (FY2001 $)	177	305
Escalation factor to FY2008	-	1.21
Total (FY2008 $)	-	370

TABLE XI: Approximate cost of a Super B Factory escalated to FY2008.

FUTURE STUDIES

Many studies must be done to bring these ideas closer to a practical accelerator. A few of the more important topics are: 1) the effects of the short beam lifetime and continuous injection on the physics detector, 2) the interaction region layout with round beams, higher detector fields and smaller IP chamber , 3) an alternate flat beam interaction region, 4) the longitudinal beam stability at high currents, 5) the parameters of the bunch-by-bunch feedbacks, and 6) the beam-beam interaction allowing a higher beam-beam tune shift but with a shorter beam lifetime.

Super*BABAR*: A 10^{36} Detector

The background rates and radiation dose to detector systems at a 10^{36} collider are such that current generation devices such as *BABAR* or BELLE could not cope; all systems must be replaced with new technology[69].

While it is possible to retain the flux return and superconducting coil of *BABAR*, all other systems would have to be replaced. To illustrate the principles governing the choice of technologies for a detector capable of doing physics at 10^{36}, we will describe a new *straw man* detector, optimized at the summer study level, for the physics, background and radiation environments of a 10^{36} collider. Figure 14 shows a representative detector design.

The scale of the detector is set primarily by calorimetry requirements. Anticipated background rates and radiation doses make it necessary to replace *BABAR*'s CsI(Tl) electromagnetic calorimeter with a device that is both more radiation resistant and faster. An intensive R&D program will be required before a final choice of calorimeter can be made. Leading candidates include a pure liquid krypton device and several types of scintillating crystals. One possibility is LSO, which is quite radiation hard and has other desirable characteristics: a short decay time, a short radiation length and and a small Molière radius.

Since precise measurement of the branching ratios $B^0 \to \pi^0\pi^0$ and $\overline{B}^0 \to \pi^0\pi^0$ is a primary goal of Super*BABAR*, good π^0 mass resolution at high momentum is a principal design criterion. We require the resolution to be at least as good as in current detectors, which translates into a requirement on angular resolution for reconstructed photons: we can scale the inner radius of the calorimeter barrel by the ratio of the Molière radii of CsI(Tl) and LSO, placing the inner radius of the barrel at 60 cm and setting the scale for other detector components.

After a discussion of the experimental environment, each of the systems will be briefly discussed in turn.

BACKGROUNDS AND RADIATION

Machine-related backgrounds present serious constraints on the design options for detector hardware, readout electronics, and the trigger system as well as on the interaction region itself. These backgrounds impact trigger rates, limit the lifetime of hardware and electronic components due to radiation damage, and affect the performance of the hardware and software associated with each detector subsystem due to extraneous signals.

The main sources of ionizing radiation at PEP-II are synchrotron X-rays produced in magnets near the interaction region and scattering of the beam with residual gas (via bremsstrahlung and Coulomb interactions) within the vacuum chambers throughout the storage ring. As the luminosity is increased, backgrounds associated with the beam-beam tune shift and luminosity are becoming more important[70]. At a 10^{36} luminosity B factory, with extremely high beam currents and short beam lifetimes,

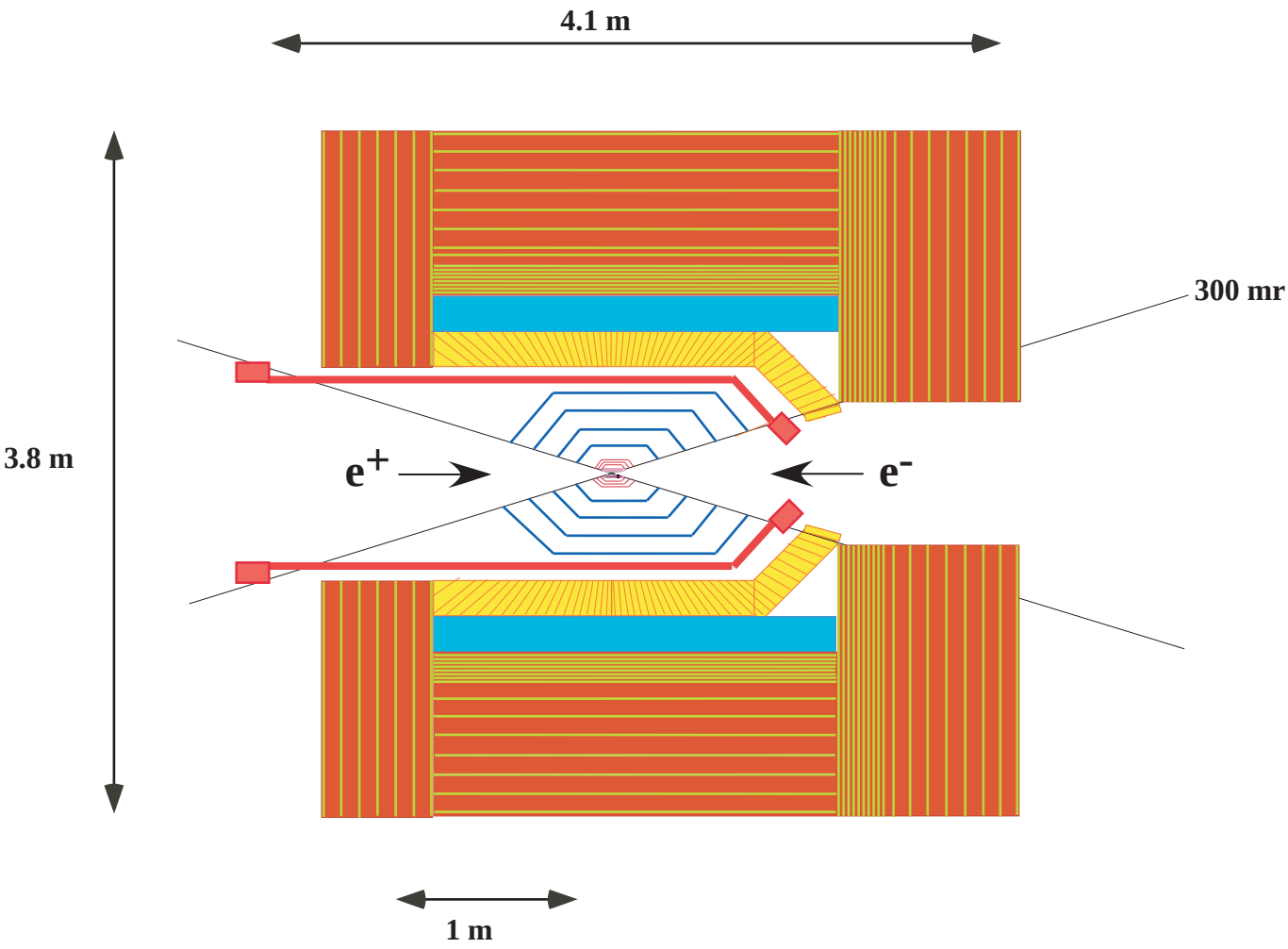

FIG. 14: Elevation view of Super*BABAR*, a detector designed for a 10^{36} collider.

it is anticipated that additional sources will also contribute.

Sources of potential beam backgrounds can be inferred from particle loss rates associated with the beam lifetime parameters for the SuperHER and SuperLER beams. Table XII compares the present PEP-II loss rates with the anticipated rates for a 10^{36} machine as described in reference [62]. In general, the relative background sensitivities to each source of lost beam particles will depend on the details of the machine optics, and the IR and detector design. It is therefore not possible to estimate the magnitude, rate and distribution of beam backgrounds in Super*BABAR* without a more complete design and simulation of the IR and machine optics. However, some educated extrapolations of background rates and radiation dose can be made using beam background measurements from *BABAR*. In *BABAR*, the presently observed beam backgrounds have been entirely attributed to only vacuum and luminosity sources, however the large loss rates due to Touschek, beam-beam and dynamic aperture for SuperPEP-II suggest that these sources will also contribute significantly.

Estimation of calorimeter rates

Estimates of background rates due to vacuum losses can be obtained by scaling the measured rates in *BABAR* by the expected loss rates at 10^{36} under the assumption that the sensitivities will be similar for the two machines. This assumption is somewhat suspect due to the expected significant differences in the beam optics, aperture limitations and the collimation scheme and therefore estimates obtained in this way are probably valid to only within an order of magnitude or so. Alternative estimates can be obtained by scaling by the beam

	HER	LER	SuperHER	SuperLER
Beam current (A)	0.7	1.4	5.5	20.5
Beam lifetime τ_b (min)	550	150	4.2	3.2
Beam loss rate I_b/τ_b (A/min)				
Luminosity			0.37	0.35
Vacuum (Brem/Coulomb)			0.06	0.68
Touschek			0.06	2.28
Beam-beam tune shift			0.55	2.05
Dynamic aperture			0.28	1.03
Total	1.3×10^{-3}	9.3×10^{-3}	1.32	6.39

TABLE XII: Expected beam loss rates for a 10^{36} collider in the PEP-II tunnel at SLAC based on the parameterization in reference [62].

currents rather than the loss rates, yielding somewhat lower background rates. This method, however, is even more suspect. Touschek backgrounds are expected to behave similarly to the distant bremsstrahlung contribution to vacuum background sources and therefore estimates of calorimeter rates can be obtained by assuming similar sensitivities as vacuum sources. No attempt has yet been made to estimate contributions from dynamic aperture and beam-beam sources, but it is expected that they could be comparable to backgrounds from other sources.

For the purposes of this work only the calorimeter backgrounds have been estimated since it is expected that beam backgrounds will significantly influence the calorimeter design for Super*BABAR*. Rates for other subdetectors will likely scale in a similar manner, and so this study should set the scale for future studies, once more detail is know about the IR and beam optics, specific to those detectors.

Since calorimeter segmentation, radial distance of the crystals from the IP, and readout speed will all potentially be different from the *BABAR* EMC, the figure of merit for calorimeter backgrounds is the total energy per unit time from backgrounds deposited within the geometric acceptance. At *BABAR* this can only be measured for energy exceeding the $\sim$ 1 MeV hardware threshold, and the relevant EMC time window for a cyclic trigger is approximately 1.85 μs.

Random trigger samples from dedicated *BABAR* single-beam and colliding beam experiments were used to obtain estimates of the detector rates attributable to vacuum and luminosity background sources. Again with all the caveats associated with extrapolating to a different machine and detector, the HER and LER background rates can be scaled to SuperPEP-II operating conditions. The results are listed in table XIII. Note that the *Physics* term refers to the contribution from triggerable e^+e^- interactions within the detector acceptance, while the *Lumi* contribution refers to the flux of low energy photons from small-angle Bhabha events in which the final state particles strike machine elements and shower into the detector. Obviously both of these terms scales with the luminosity. The *Lumi* contribution is presently quite large and not well measured, but could presumably be significantly reduced in Super*BABAR* through appropriate IR design.

The estimated injection currents for PEP-II are typically $\sim$ 150 mA/min per beam. For SuperPEP-II, the injection current by definition must be equal to the beam loss rate (1.32A/min HER; 6.39A/min LER). A naive scaling factor would then be something like $7.7/0.150 \sim 50$. By examining the *BABAR* EMC and SVT the average backgrounds during injection were estimated to be a factor 3-5 times worse than the rates during stable beams running. The overall injection rates for SuperPEP-II are therefore expected to be a factor $\sim$ 150 larger. This translates into an additional $\sim$ 120 GeV/1.85 μs in the calorimeter.

In total a rate of one or two hundred GeV per 1.85 μs over the entire EMC is possible, compared to the 1-2 GeV per 1.85 μs for *BABAR*. To reduce this to a reasonable level will require substantially faster detector components in Super*BABAR*.

Calorimeter Radiation Dose

In its first 23 fb^{-1} of operation, the *BABAR* EMC integrated $\sim$ 200 Rad in the forward direction and $\sim$ 100 Rad in the backward direction. The inner rows of the EMC endcap are not only directly in the path of photons from a number of background sources, but are also physically closest to the beam pipe. The radiation dose rates in the current EMC endcap crystals are therefore probably reasonable values to use for conservative dose extrapolations. Assuming that the instantaneous dose is approximately proportional to the total energy per event which is deposited in the EMC, then the dose due to *Lumi* is comparable to the dose from the HER and LER single beams. If the entire observed dose in the hottest region of the detector is then attributed in turn to the HER, LER and *Lumi* sources, the expected maximum doses rates for SuperPEP-II can be estimated. These estimates are

Source	*BABAR*		Super*BABAR*	
HER (Vacuum)	620 mA	~ 380 MeV	5.5 A	$3.4 - 18$ GeV
HER (Touschek)		-		$\mathcal{O}(10$ GeV)
LER (Vacuum)	1200 mA	~ 480 MeV	20.5 A	$8.2 - 35$ GeV
LER (Touschek)		-		$\mathcal{O}(100$ GeV)
Lumi	2×10^{33}	$0.6 - 1.3$ GeV	1×10^{36}	$300 - 650$ GeV
Physics	2×10^{33}	< 5 MeV	1×10^{36}	~ 1.3 GeV
Injection	-	-	1×10^{36}	~ 120 GeV

TABLE XIII: Total energy attributable to beam backgrounds deposited in the entire EMC per 1.85 μs timing window. Backgrounds from beam-beam and dynamic aperture beam losses have not been estimated but are expected to also contribute significantly.

listed in Table XIV, where the expected dose is on the order of hundreds of kRad per year.

The EMC at present receives very little radiation dose from injection. In contrast, operational experience with *BABAR* and PEP-II has shown that roughly equal amounts of radiation dose are received in the innermost detectors from injection and stored beams. To estimate the dose from continuous injection at SuperPEP-II the present instantaneous background rates can be scaled by the injection currents. Assuming a factor of 150× the *BABAR* single beam contributions as before, the injection dose rate is then estimated to be $\sim$ 50 kRad/year. Of course, if the inner radius of the Super*BABAR* calorimeter is different from *BABAR*, these values will need to be scaled appropriately.

Source	*BABAR* (Rad/year)	Super*BABAR* (kRad/year)
HER (Vacuum)	≤ 200	$2 - 10$
HER (Touschek)	-	$\mathcal{O}(10)$
LER (Vacuum)	≤ 200	$3 - 15$
LER (Touschek)	-	$\mathcal{O}(50)$
Lumi	≤ 200	≤ 100
Injection	(small)	$\mathcal{O}(50)$

TABLE XIV: Estimated radiation dose in the calorimeter per year of operation. The contribution to the total dose from beam-beam and dynamic aperture backgrounds has not been estimated.

RADIATION MONITORING AND PROTECTION

A key ingredient to consistently achieving high integrated luminosities for *BABAR* has been efficient radiation protection. The incorporation of an effective radiation protection and monitoring system must therefore be recognized as a key element of the detector early in its design. The most vulnerable parts of the detector are likely to be the silicon and gas trackers and the calorimeter.

In *BABAR*, a system of 12 large-area PIN diodes with direct coupled readout has provided a versatile protection and monitoring system. PIN diodes were chosen because they uniquely meet the extremely tight space requirements and are a natural match to the sensitive silicon material in the vertex tracker. However, radiation damage during long storage ring fills and annealing of damage between fills are starting to affect the large temperature-dependent leakage current to such an extent that the signal is very difficult to interpret. An AC-coupled readout would have the advantage of only measuring the radiation-induced signal but would require a sophisticated design capable of resolving a high rate (many MHz) of weak pulses. For higher-luminosity machines with the expected higher radiation dose rates, PIN diodes might not be a viable solution.

Given the space constraints and the difficulty in designing specialized readout electronics, serious consideration should be given to using the detector subsystems themselves as elements of the radiation monitoring and protection system. One constraint that this introduces is that any detector subsystem that provides radiation protection must be active any time there is beam in the storage ring, including machine-development periods.

TRIGGER, DATA ACQUISITION AND COMPUTING

Triggering at 10^{36}

The potential physics goals for a 10^{36} Super*BABAR* lead to a strong preference for an *open* triggering scheme, highly efficient for virtually all B meson decay modes. Such open triggers have been the norm at e^+e^- colliders, in contrast to the highly selective triggers used at hadron colliders. Although the trigger and data acquisition rates at SuperPEP-II are comparable to current hadron colliders, the use of an open trigger is necessary for the physics at the $\Upsilon(4S)$. We believe that it is possible to design a data acquisition, reconstruction, and analysis system meeting this goal using technologies already in hand or reasonably foreseeable to become available on the relevant time scale.

Many of the physics topics discussed involve analysis of particles recoiling against fully or partially reconstructed

B decays. This will require accumulating the largest possible sample of such decays, a goal that is clearly incompatible with a narrow trigger designed to select only certain decay signatures. Conceivably, if only a small number of distinctive recoil decay modes were of interest, a trigger could be devised that operated on their distinguishing features. However, we believe it would be challenging to achieve this while meeting the performance, reliability, and modelability requirements. Moreover, it does not appear that all the rare signal decay modes of interest do in fact offer readily triggerable signatures. One of the great advantages of a e^+e^- facility compared to a hadronic machine inherently is in the ability to trigger on virtually all B decay modes with high efficiency, and we believe this advantage is worth exploiting.

Luminosity and physics cross-sections

At the $\Upsilon(4S)$ center-of-mass energy the total cross-section, including radiative corrections, is about 2.09 nb for continuum production of $u\bar{u}$, $d\bar{d}$, and $s\bar{s}$, 1.30 nb for continuum $c\bar{c}$, 0.94 nb for $\tau^+\tau^-$, and 1.04 nb for $\mu^+\mu^-$. For a beam energy spread comparable to that of PEP-II, the cross-section for $B\bar{B}$ pairs from the $\Upsilon(4S)$ is about 1.05 nb.

The Bhabha differential cross-section varies strongly with angle near the forward direction, so the total triggerable cross-section is a sensitive function of the acceptance of the detector in this region. For *BABAR*, it has been determined to be approximately 50 nb. The Super*BABAR* design envisions maintaining the same 300 mr cone for accelerator components near the beam line, so we assume that the effective Bhabha cross-section detector will be comparable to that for *BABAR*.

At the design luminosity of one $\mathrm{pb}^{-1}\mathrm{s}^{-1}$, each nanobarn of cross section results in 1000 events per second.

Trigger Rates

The scaling of the *BABAR* trigger and the associated data acquisition upgrade issues have been considered in detail for luminosities up to $3 \times 10^{34}\mathrm{cm}^{-2}\mathrm{s}^{-1}$. We extend those methods to $\mathrm{L} = 10^{36}$, taking into account the beam currents and available background estimates for the strawman collider design. One crucial assumption is the ability to build a tracking trigger for the all silicon tracker being considered.

The trigger has two levels: one hardware-based (*Level 1*) which operates on a set of coarse-grained *trigger primitives* constructed from information from the drift chamber and the electromagnetic calorimeter, and one software-based (*Level 3*) which operates on complete events and uses the full information available from the same two detector systems.

Hardware trigger level

At the present PEP-II luminosity of 3.3×10^{33}, the hardware trigger produces about 1000 triggers per second (Tps), from a combination of beam-gas and beam-wall backgrounds, which scale with beam current, and luminosity-related events. Current projections based on the upgrade plans for PEP-II show that at luminosities above 10^{34} the hardware trigger rate will be dominated by interactions that scale with luminosity. Continuing the projections further, to 10^{36}, the rate for a *BABAR*-like hardware trigger would be expected to be about 72 kTps. About 40–50 kTps of this would be attributable to Bhabha interactions. The rate due to beam background would be only about 8 kTps. (Most of the remainder is believed to arise from low-mass two-photon interactions.)

Although we can anticipate that the beam backgrounds may be worse in the Super-B-factory, notably because of the continuous-injection design, based on these estimates any such increases will be starting at a small fraction of the total trigger rate.

In extrapolating from the present *BABAR* situation, it is important to recall that the current hardware trigger does not make use of information from the drift chamber about the axial (z) component of charged particle trajectories. A trigger capable of doing this well would be able to eliminate most beam background events, in which the tracks produced generally originate away from the primary beam interaction vertex either in z or in the transverse plane.

We also believe that it should be possible to devise a way to identify and veto some fraction of particularly clean Bhabha interactions in the hardware trigger.

However, for the purposes of this note, we will take a very conservative approach and consider the practicality of supporting a hardware trigger running at up to 100 kTps.

Software trigger level

We define this level as continuing through the point at which the last irreversible decision is made whether or not to save an event to permanent storage.

In the *BABAR* experiment, a rather loose selection is applied at this stage at present, resulting in a rate of about 100–150 Tps saved to archival storage at current luminosities, including calibration triggers of various sorts (e.g., prescaled pass-throughs of unfiltered hardware triggers).

In *BABAR*, a further stage of filtering is applied offline, in which it is decided which events are to be passed on for full reconstruction. The core of the filter is a requirement for at least three charged tracks, reconstructed by

a more accurate, but slower drift chamber-based algorithm than used in the trigger, augmented by specialized filters designed to recover low-charged-multiplicity B decays. Presently this filter passes an effective cross-section of 6 nb for physics processes, in addition to a small subsample of the calibration triggers. The total cross-section for multihadron-like d, u, s, c, τ, and b events observable in the *BABAR* detector is about 4.65 nb, so this filter is still passing a considerable rate of additional events, believed to arise primarily from two-photon processes, and could almost certainly be tightened further.

We will proceed based on the assumption that a filter with a total effective cross-section of 6 nb will be feasible. This presumes a modest improvement in the physics selection over the present *BABAR* filter, maintaining full efficiency for B meson decays, and high efficiency for the charm continuum and for $\tau^+\tau^-$ events with at least four charged tracks, combined with a prescaled selection of two-prong events of interest. We envision that an equivalent of such a filter would be included in the software trigger level of the data acquisition system for the Super-B-factory detector.

Maintaining the 6 nb cross-section in that environment would depend on whether higher background occupancies would lead to a significant likelihood of the presence in any given data acquisition window of reconstructable charged tracks or calorimeter energy clusters. The danger here is the possible promotion of events from otherwise readily eliminated low-multiplicity but high-rate categories, most importantly Bhabha and radiative Bhabha events, to the higher-multiplicity hadronic physics categories. Evaluating the likelihood of this effect would be a necessary element of further preparatory studies for the Super-B-factory detector.

Data Acquisition and Logging

Estimates of the hardware trigger rate, as discussed above, are in the range of 10–100 thousand of triggers per second. Data acquisition at these rates is certainly technically challenging. Avoiding irreducible per-trigger dead time, in particular, will be important. For *BABAR*, this parameter is 2.6μs; this would have to be reduced to less than 0.1μs for the Super-B-factory detector, or eliminated altogether, in order to avoid degrading DAQ efficiency.

It is important to remember that the LHC's ATLAS and CMS detectors will already have achieved equal or better performance by the time the Super*BABAR* detector would be under construction. Prototype electronics for ATLAS and CMS is already in existence, meeting most of those experiments' requirements. In this report we rely on this suggestion that this part of the problem can be solved and we have not attempted a front-end electronics design at this time.

We discuss briefly how the downstream components of the data acquisition system might be realized. The basic design principle is to maintain parallelism as much as possible throughout the system, from front-end data acquisition through software triggering, data logging, reconstruction, and analysis, eliminating single-path bottlenecks to the greatest extent possible. This principle will need to be applied more thoroughly at the Super-B-factory than before. *BABAR* and BELLE, for instance, log data to a single server; we would not expect to be able to do so. Parallelized data logging has been demonstrated in other high energy physics experiments such as NA–48. We also anticipate that highly parallel approaches to all phases of data analysis will be needed in order to handle the data volume.

Event size

Controlling the event size at the Super-B-factory detector will probably present another of the greatest challenges in the design of its data acquisition system, largely because of the consequences for the total volume of data to be archived and the cost of the media involved.

Simple scaling of the *BABAR* event size (presently about 28 kB per event accepted by the software trigger) to the Super-B-factory is inappropriate, as significantly different detector technologies are envisioned to be used. However, we note that the *interesting* information content of hadronic events should not be significantly different from that for *BABAR* — the same types of physics data are being acquired, and the number of measurements made per charged or neutral particle is not expected to be very different.

For this reason, we make one ambitious assumption: that the event size can be limited to 50 kB, roughly doubling the *BABAR* size. Achieving this goal will require, relative to *BABAR*, more ambitious suppression of single hits from background occupancy and more effective compression of data to be transmitted.

We assume that the software trigger will add 5 kB of information to the raw event detailing the results of its processing (in effect, a partial reconstruction pass). Following reconstruction, we assume event sizes of 1 kB for *tag* data to be used for indexing events, and 6 kB for *DST*-level information. We anticipate that full reconstruction output will not be saved to permanent storage for every recorded event, but rather generated on demand, and perhaps saved for small, specific subsamples of the data.

Event building

The full data volume sent to the software trigger, under the above assumptions, is 100,000 Tps $\times$ 50 kB = 5 GB/s.

We envision a hierarchical networked event builder similar to *BABAR*'s. In this model the full data rate appears only in the final network switch at the top of the hierarchy. Since switches with 64 Gbps backplanes are already available today, this should not present a problem.

We assume 100 software trigger machines analogous to today's high-density rack mount compute servers. Again, we foresee no problem in moving 50 MB/s of data in, and 3 MB/s out. This is already possible with Gigabit Ethernet, which is on the verge of being a commodity technology now. Today's typical high-end Linux machine can readily saturate a Gigabit link using the UDP protocol (in fact, 1.5 Gbps has been achieved over two links in tests at SLAC), and with further improvements in hardware support of the network stack we expect the CPU cost to drop further.

Running the software trigger

The empirical Moore's Law-like scaling factor observed at SLAC and CERN suggests a factor of 50 in CPU capacity versus today's machines would be achieved by 2008. Today's machines, in turn, are about 2.5 times faster than those currently in use in the *BABAR* software trigger. In order to be conservative, however, in the analysis below we use a net scale factor of 100, not 150. Note that we do not depend on per-CPU speed increases of this magnitude, only on the total compute capacity of each commodity farm node. If this takes multiple CPUs per box, that presents no additional problems.

On a 100-node farm, given the trigger rate and cross-section assumptions above, each node would process 1000 input events per second and accept 60 of them.

We assume a two-stage software trigger. The first stage is taken, *very* conservatively, to be identical in its effective cross section to the present *BABAR* software trigger. That trigger currently runs at 75 events per second per node. We derate this by a factor of two to account for the larger expected event size, then scale up by the CPU speed factor of 100, yielding a per-node rate of 3750 Tps. So, the actual load of 1000 Tps uses 27% of each node's capacity. Scaling from the *BABAR* trigger behavior, we expect a 200 Tps rate to be accepted by this stage.

We then apply a further trigger level analogous to *BABAR*'s present offline filter, discussed above. On each machine, we have 3.6 ms of time available to process each event — 360 ms in current *BABAR* farm units. The *BABAR* filter currently requires O(1s) for this task. However, it has not been aggressively optimized for speed. (A relevant comparison point is that the 1996 CLEO *full reconstruction* took 250 ms/event on comparable machines.) We think it highly plausible that this goal can be met. If not, this is a very scalable system and more nodes can certainly be added.

We anticipate no memory bandwidth problems in handling the data.

Data Logging

The data volume out of the software trigger is 6000 Tps $\times$ 55 kB = 330 MB/s. Moving this data off the machines presents no problem. Logging will have to be done in parallel. We anticipate that tape-like devices capable of handling 15–20 MB/s will be affordable, and we would require about 20 of these. The tape media presently used by *BABAR* hold 60 GB. Assuming no change to this, we would fill one tape every three minutes or so, a rate easily handled by present tape robots.

BABAR's present tape silos provide about 415 TB/$M, all associated hardware costs included. The empirical bytes-per-unit-cost scaling observed at SLAC and CERN has a doubling time of about 2.1 years. Scaling from 2000 to 2008 we get a factor of 14, or 5800 TB/$M. This corresponds to a media cost for the Super-B-factory raw data of about $600K / Snowmass year which, while high, seems acceptable.

Offline Computing

Offline Computing refers to all those computing activities after the data has been acquired and written to permanent storage. Reconstruction, Monte Carlo simulation, skimming, and physics analysis represent the greatest loads. It is not our intention to present a solution, optimized or otherwise. Rather, we wish to show that the scale of the problem is manageable.

There are two experiments at high-luminosity B-Factories in operation today: *BABAR* and Belle; both are running at luminosities of $3-4\times10^{33}$. Their computing loads are very similar. It takes 5 seconds to reconstruct a hadronic event on a 1-GHz P-III CPU, while simulation and reconstruction together take 7 seconds. The central computing resources of Belle were recently upgraded after five years, and demonstrated the ability to reconstruct 1 fb^{-1} per day. *BABAR* computing has more frequent but smaller upgrades. The current setup has reconstructed 0.5 fb^{-1} per day. In addition, the *BABAR* collaborators in the U.K. expect a new compute farm to be operational later this year, with the capacity to simulate and reconstruct 1 fb^{-1} of hadronic events per day.

When considering computing capacity, it is more useful to consider integrated luminosity rather than peak luminosity. The new experiment is expected to record 10 ab^{-1} per year. Assuming 200 running days, a capacity of 50 fb^{-1} per day is needed for reconstruction to keep up with data taking. This is approximately 50 times the demonstrated capacity of Belle. Storage requirements also scale with integrated luminosity. Hence, we expect

to need 50 times the capacity as currently needed. Historical trends suggest that the unit cost of computing goes down by a factor of 2 every 18 months. Thus, we can expect 40x improvement in performance per unit cost by 2009. Obtaining 50x in performance can be achieved at a cost similar to today's B-Factories. Note that we are concerned here with cost performance scaling, and not the performance of a single CPU.

VERTEX RECONSTRUCTION AND TRACKING

Due to the intense rates expected at a luminosity of 10^{36}, a conventional drift chamber would likely experience 100% occupancy. Therefore a tracking detector must have several orders of magnitude greater segmentation and time resolution. A silicon tracking detector has been considered for the Super*BABAR* strawman design.

In particular, we have studied a tracking detector compatible with the high field, compact design which consists of two layers of silicon pixel detectors and seven layers of double-sided silicon strip detectors. The dimensions and radial positions of the detectors used for a study of tracking resolution are shown in Table XV.

The magnetic field is taken to be 3T. For the initial study, the multiple scattering in each layer is assumed to be that due to 300 μm of silicon. The beam pipe has a 1.0 cm radius and a thickness of 0.7% radiation lengths. For pions produced perpendicular to the field in the laboratory, the transverse momentum resolution has been studied using a Monte Carlo simulation of hit positions generated using multiple scattering and detector resolutions based on pixel and strip sizes only, assuming digital readout rather than analogue. The generated hits are fit using a Kalman filter algorithm to determine momentum at the beginning of the track.

The results of this study are shown in Table XVI. For tracks with transverse momentum greater than 400 MeV/c the resolution can be characterized roughly as $\sigma_{p_T}/p_T = (0.48 + 0.024 \times p_T(\mathrm{GeV}/c)\%$. For comparison, parameterizing the corresponding results found in the *BABAR* TDR gives $\sigma_{p_T}/p_T = (0.2 + 0.12 \times p_T(GeV/c)\%$. Below 400 MeV/$c$ tracks traverse a smaller number of detector planes, so the resolution becomes much worse very quickly. If we double the number of radiation lengths of the detectors to account for mechanical support structures and electronics, the resolution for tracks with $p_T > 400$ GeV/c can be characterized roughly as $\sigma_{p_T}/p_T = (0.70 + 0.019 \times p_T(GeV/c)\%$. These resolutions are somewhat worse than those in *BABAR*. They can be improved by using analogue readout for some of the strip detectors, as is done in *BABAR*. Further study is need to allow for optimizing the number of layers and their locations.

PARTICLE ID

There are two distinct B physics studies requiring particle identification capability in differing momentum regions :

- the separation of pion and kaon daughters in charmless B decays in the range 1.5 to 4 GeV/c with the current boost of 0.6, or to 6 GeV/c if the boost is increased to 0.8.
- B^0 and $\overline{B}^0$ flavor tagging with kaons , via the $b \to c \to s$ cascade; momenta are typically less than 2 GeV/c.

Other physics analyses, for example those involving charm and τ studies, can effectively take advantage of better performance in pion/kaon separation at even higher momenta. We will strive to provide better performance (*i.e.,* higher momentum limits for pion/kaon separation) than we have in the current *BABAR* DIRC particle identification system.

We propose providing this high momenta particle identification information through an upgraded DIRC system, while relying on supplementary information at lower momenta. At the lowest momenta (*i.e.,* below $\sim$ 400 MeV/c) we expect good dE/dx information from the silicon tracking device. A time of flight system could provide particle identification up to 800 or 900 MeV/c. This should provide excellent particle identification capability up to the DIRC cut-off for the new detector, see Figure 15.

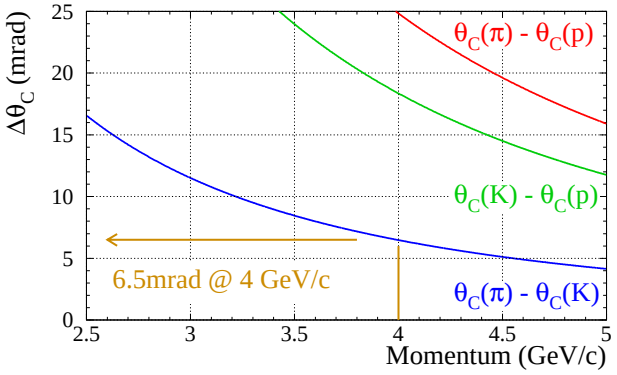

FIG. 15: Cerenkov angle difference versus momentum.[71]

The proposed new DIRC system employs quartz bars as the radiators, as in the original DIRC, but couples the Cerenkov light trapped within the bars by internal reflection to compact photo-detectors using quartz lens/mirror focusing elements. This allows for the removal of the large water stand-off box, consisting of 10 tons of pure water, that would become a serious background source

Layer	Type	Radius
1	50 μm × 150 μm pixels	1.3 cm
2	50 μm × 150 μm pixels	1.8 cm
3	3 mm long, 50 μm pitch, double-sided strips	3.0 cm
4	3 mm long, 50 μm pitch, double-sided strips	6.0 cm
5	3 mm long, 50 μm pitch, double-sided strips	9.0 cm
6	3 cm long, 50 μm pitch, double-sided strips	15.0 cm
7	3 cm long, 50 μm pitch, double-sided strips	25.0 cm
8	3 cm long, 50 μm pitch, double-sided strips	35.0 cm
9	3 cm long, 50 μm pitch, double-sided strips	45.0 cm

TABLE XV: The arrangement of tracking detectors used to study tracking resolution in the compact detector with a 3T magnetic field.

p_T (MeV/c)	σ_{p_T}/p_T (%) base model	σ_{p_T}/p_T (%) double thickness	σ_{p_T}/p_T (%) *BABAR* TDR
50	4.0	4.3	
100	2.25	3.1	
200	0.66	0.94	
400	0.52	0.72	0.25
800	0.50	0.72	0.30
1600	0.52	0.73	0.39
3200	0.54	0.76	0.58
4000	0.58	0.78	0.68
5000	0.60	0.80	0.80

TABLE XVI: Transverse momentum resolution for pions produced perpendicular to the magnetic field in the detector model of Table XV, using a 3T field. The models for multiple scattering and detector resolution are described in the text.

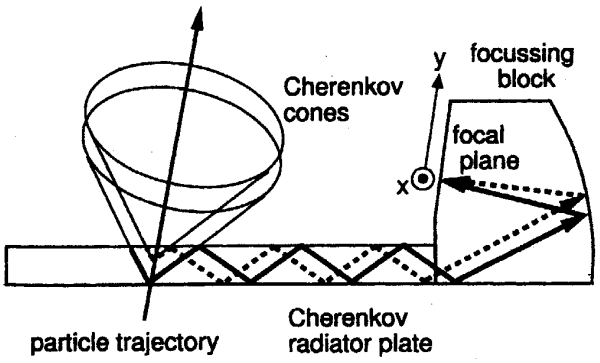

FIG. 16: Schematic layout of a single quartz bar radiator complex.

for the 10^{36}, as well as for improved spatial and time resolution performance.

The performance of the DIRC is captured in the relationship :

$$\Delta\theta^2_{\check{C}}(\text{photon}) = \Delta\theta^2_{\check{C}\text{tracking}} + \Delta\theta^2_{\check{C}\text{dispersion}} + \Delta\theta^2_{\check{C}\text{transport}} + \Delta\theta^2_{\check{C}\text{imaging}}$$

$$\Delta\theta_{\check{C}}(\text{track}) = \frac{\Delta\theta_{\check{C}}(\text{photon})}{\sqrt{N_\gamma}}$$

The performance of the detector is dominated by the imaging term ($\sim$ 7 mrad per photon detected) and the dispersion term ($\sim$ 5.4 mrad per detected photon). By using a quartz coupling focusing element (Figure 16) the large imaging term is reduce by a factor of three to four. By employing new, fast photo-detectors, with less than 200 ps timing capability, one hopes to reduce the dispersion term by about a factor of three. This should result in an upgraded DIRC performance of about 2.7 mrad resolution per detected photon, or about three times better than the existing DIRC detector.

The particle identification system also includes a forward DIRC (Figure 17), with readout from the inner edge, providing fast π/K identification in the region (350 mrad to 2800 mrad)

An R&D program to investigate the performance of new photo-detectors with appropriate quantum efficiency, geometrical resolution and timing capability is being carried out at SLAC. Simulation studies of different focusing geometries are also underway. The new device should be radiation resistant to dose rates in excess of 100 kRad, which is satisfactory for this environment.

The backgrounds at the high luminosity B Factory will be quite different, and will require serious studies, including learning from the continuous injection experience of SLD at the SLC, and from new measurements taken at *BABAR* with continuous trickle injection to PEP-II. From current studies it appears that with fast photo-detectors (with better than 200 ps performance) the new upgraded DIRC system should be able to handle this demanding new environment.

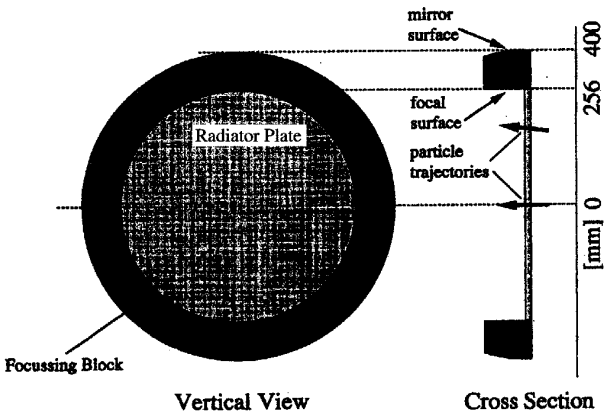

FIG. 17: Schematic of a forward DIRC.

CALORIMETRY

Overview of Performance Issues

We expect that a crystal calorimeter will again likely be the technology of choice for Super*BABAR*. As will be shown in the subsequent sections, the principle areas of concern are the impact of beam and luminosity backgrounds on the calorimeter performance, and ultimately, the radiation hardness of the device.

These problems must be addressed in such a manner that the quantitative performance goals of the calorimeter are still achieved. Very roughly, we wish to achieve *BABAR*-TDR like performance parameters, as shown in Table XVII

	Design Goals
σ_E/E	$1\%/E(\mathrm{GeV})^{1/4} \oplus 1.2\%$
σ_θ	3 mr$/E(\mathrm{GeV})^{1/2} \oplus 2$ mr
ϵ_γ at $E_\gamma \sim 100$MeV	$> 95\%$
ϵ_γ at $E_\gamma \sim 20$MeV	$> 85\%$
E_γ(min)	~ 10MeV
e/π separation ($\epsilon \sim 95\%$)	$\sim 10^{-3}$
Geometrical Acceptance	$> 95\%$
Dynamic Range	18 bits

TABLE XVII: Design goals for the *BABAR* CsI(Tl) calorimeter. Values for efficiencies are at normal incidence.

In addition, the calorimeter should be relatively easy to calibrate and should be very stable over time against the environment. Finally, reliability of components is extremely important to achieve hermeticity of the device. This feature becomes more and more important as we seek to measure rarer and rarer processes.

Backgrounds and Radiation

Radiation damage to scintillating crystals leads to a reduction in total signal as well as non-uniformities in longitudinal response leading to energy dependence of response. The overall response change as a function of energy can be measured and removed *on average*, but shower fluctuations will always result in the sampling of residual non-linearities which appear in the constant term of the energy resolution. Radiation damage for example in CsI(Tl) results in color center formation at the front of the crystal, which reduces the transmission of light in the crystal. Accordingly, geometrical changes to the crystal and readout may reduce the impact of damage.

Estimates of calorimeter beam background rates and radiation dose are presented in the preceding section. These results suggest that the calorimeter will require crystal and readout features which are significantly beyond the existing *BABAR* design utilizing CsI(Tl) and coarse waveform sampling/digital filtering readout. The expected requirements are

a) Reduction of the effective visible backgrounds in triggered events by a factor of 250× to 500×.

b) Radiation hardness at a level of > 50 kRad/yr to ~ 100 kRad/year

Item (a) implies that one must likely go to shorter decay time crystals (one might get a factor of 50× as will be seen in the next sections). Timing information on the signals might give another factor of 10× improvement (*BABAR* currently employs a ±125 ns window on calorimeter signals). Some additional granularity might also help. Alternately, one must use significantly more sophisticated waveform sampling, digital filtering, and pattern recognition techniques although the experience of *BABAR* would lead one away from this direction.

Item (b) implies that one must go to considerably more radiation hard crystals, and/or consider a scheme where the crystals are segmented longitudinally and perhaps laterally (see Figure 18) to reduce the impact of radiation damage on the signal light yields and non-uniformities induced by the radiation damage.

Calorimeter model

A number of different calorimeter models are being considered, but only a compact detector model is discussed here. In this model we shrink the detector volume, allowing the use of material having a generally higher cost/cc. Specifically, we consider the elimination of the use of (unshielded) gaseous detection elements such as a conventional uni-volume drift chamber on the assumption that backgrounds and radiation from the beams and

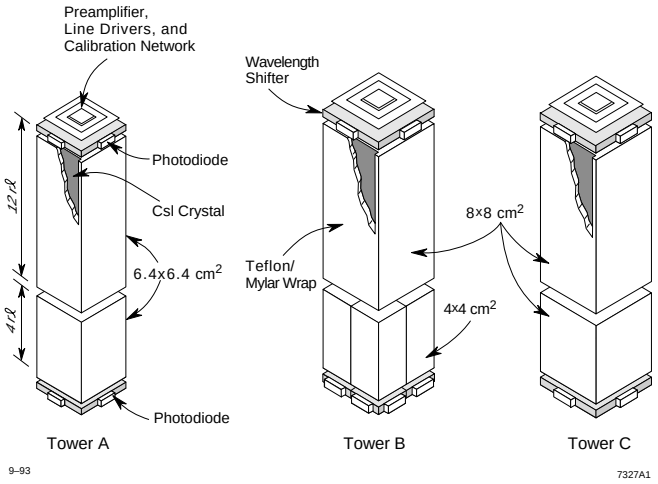

FIG. 18: Example of a longitudinally segmented readout tower scheme[72]

injection will be too high to operate. We assume that the tracking is all done in a compact silicon device in a high field magnet, or perhaps some hybrid of silicon and small diameter straw tubes. Calorimetry would then start at a smaller radius. The impact is ideally to require a crystal with smaller Molière radius, shorter radiation length, and/or finer segmentation. The coil would be placed directly outside the calorimeter, and a higher field would be needed to compensate for the smaller tracking volume. Calorimeter readout would need be immune to the field, implying photodiode or other solid state device with gain (perhaps avalanche photodiodes). A longitudinally fine-grained muon system could be integrated into the flux return, or hybridized as well. The calorimetric difficulties of all compact detectors are:

a) maintaining position resolution sufficient to overcome the shorter lever arm. The impact of longitudinal shower fluctuations becomes more important if the detector is at all non-projective.

b) transverse segmentation to deal with electromagnetic shower overlaps in worst case events. A small Molière radius becomes important.

c) the impact of hadronic showers whose scale is physically large for all possible materials ($\lambda_{\rm nuclear} \sim$ 20 to 30 cm) compared to the compact calorimeter size itself. The impact of overlaps must be weighed.

d) Inactive material in supports and readout must be controlled as it may represent a greater portion of the solid angle and influence the resolution.

Crystal Options

Backgrounds and radiation damage provide tight constraints on the species of crystals that might be used for the calorimeter. Characteristics of various crystals are listed in Table XVIII.

The CLEO, BELLE and *BABAR*, calorimeters use crystals of CsI doped with Tl. The characteristics of this material are shown in the first column of the Table I. The advantages of this crystal are its superb light yield, relatively short radiation length, emissions peak in the visible that allows use of silicon PIN photodiodes, and good manufacturability (low melting point, ease of machining, only mildly hygroscopic). However, this crystal is not appropriate to Super*BABAR* needs: the radiation hardness is clearly inadequate and the decay time is very long, leading to overlap of backgrounds in physics events. *BABAR* calorimetry was designed with adequate headroom in light output to allow a $\sim 20\%$ assumed light loss over its ~ 10 kRad lifetime, due to radiation damage. The average effect is correctable weekly by use of the 6 MeV source calibration and Bhabha events. CsI(Tl) was reasonably inexpensive for *BABAR*, costing only about \$3.25/cc in the almost 6 m^3 quantity.

Several crystals have properties which are potentially consistent with the expected design requirements. In particular, Cerium doped Yttrium Aluminum Perovskite (YAP) has short decay time, good Molière radius, relatively high light yield, and is radiation hard. The radiation length is somewhat large, which may have consequences for its use.

LSO has excellent radiation length and Molière radius, excellent light yield, a short decay time, and is radiation hard. Full size crystals can probably be produced. Cost at the manufacturer holding the patent on production of this material is $\sim$\$50/cc. Other producers have entered the market recently: it is not known if this has affected the price. The cost is driven partially by the cost of raw materials ($\sim$\$7/cc) and the high melting point.

The most attractive crystals from a performance standpoint are often substantially more costly than the materials that have been used in large calorimeters in the past. Many of these materials are high density, short radiation length crystals. This compensates somewhat for higher costs: the figure of merit should be related not to the cost per cc but to the cost per radiation length. The high price for these crystals argues for a more compact calorimeter, and consequently overall detector, to minimize the material cost. As was the case with $PbWO_4$, developed for CMS, it is possible that intensive development can substantially reduce the production cost of some of the attractive candidates.

Readout Options

All of the radiation hard, short decay time crystals have substantially lower light yield than CsI(Tl). Detec-

Crystal	CsI(Tl)	CsI	BGO	BaF_2	$PbWO_4$	CeF_3	YAP	GSO	LSO
τ decay(ns)	680, 3340	16	300	.6, 620	5, 15	10-30	27	56, 600	47
χ_0(cm)	1.86	1.86	1.12	2.03	0.89	1.66	2.63	1.39	1.14
$R_{\rm moliere}$ (cm)	3.8	3.8	2.3	3.4	2.2	2.6	2.8	2.4	2.3
$\lambda_{\rm nuclear}$ (cm)	37	37	22	30	22	26			
LY (γ/MeV)	56000, 64:36%	2500	8200	1400f, 9950s	100	3500	16200	12500, 1250	27000
λpeak (nm)	550	315	480	220f 310s	420-500	310-340	390	440	420
Rad Hard (Mrad)	.01	.01-.1	.1-1	1	100	1	10	100	100
ρ (g/cm3)	4.51	4.51	7.13	4.89	8.28	6.16	5.35	6.70	7.40
n_0	1.79	1.95	2.15	1.56	2.20	1.68	1.94	1.85	1.82
Cost ($ /cc)	3.2	4	4	5	8	3	?	> 15	> 7

TABLE XVIII: Potential Crystals and Their Properties

tors that selected CsI(Tl) for their calorimeter have used up to 4 cm^2 of PIN silicon photodiode to sense the emitted light. An alternative technology that has some gain will need to be used to read out the new crystal species in order to provide comparable performance. The most attractive technology is the avalanche photodiode (APD). The device is thin and compact, insensitive to magnetic fields, has a fast rise time, good quantum efficiency at short wavelengths if the structures are reversed, and a gain of about 50. APDs are radiation hard and are also less sensitive to nuclear counter effects. Consequently placement at the front of the crystal can be contemplated.

Other read out devices that should be investigated include vacuum phototriodes (VPTs) and flat PMTs (in development at Hamamatsu). The VPTs give gains of about 10-12, which drop in a high magnetic field by about a factor of two. Both APDs and VPTs are available at acceptable prices.

MAGNET AND INSTRUMENTED FLUX RETURN

The superconducting solenoidal coil of the compact detector is envisioned to provide a 3T field. The steel flux return must provide adequate cross section for the return of magnetic flux with minimal saturation, and must also provide a sufficient number of strong interaction lengths to allow discrimination between pions and muons by range. The flux return is envisioned to have a hexagonal cross section. The compact design likely obviates the need for an eight-sided design, as individual sections of the barrel weigh only about 30 tons. A four-sided device has also been considered. The total weight of the flux return is of the order of 500 tons.

Efficient detection on muons for tagging and of neutral hadrons (K_L^0 and neutrons for event reconstruction) is an important design criterion for any general purpose detector. This is conveniently done by employing a highly-segmented steel magnet flux return as is done by *BABAR* and BELLE, where the sensitive detectors inserted in the slots in the flux return are resistive plate chambers (RPC's). The *BABAR* RPC's are constructed of phenolic plates coated with linseed oil; the BELLE RPC's are made of glass.

At SuperPEP-II, the singles rates due to through-going beam particles produce singles rates in the RPC's that are likely to be unacceptably high. The sensitive detectors in this design are therefor envisioned to be plastic scintillator strips read out with wavelength-shifting fibers and multianode photomultipliers, a là MINOS.

In the compact design under discussion, the inner surface of the barrel flux return is at 1 m from the beam line. There is a total of 90 cm of steel in the flux return, *vs.* 65 cm in *BABAR*, which will result in improved π/μ separation at high momentum. The barrel is composed of 8 layers of 2.5cm plates followed by 7 layers of 10 cm plates.

The forward end cap, which is exposed to higher momentum particles, is 1m thick, composed of 18 layers: 10 of 2.5 cm, 1 of 5 cm and 7 of 10 cm. The backward endcap is 70 cm thick, composed of seven layers of 10 cm thickness.

DETECTOR COST CONSIDERATIONS

The budget for *BABAR* was baselined in November 1995. The $\sim$ \$98M cost at completion in December 1999 reflects the total detector cost employing US accounting methodology. Using the technology choices of the strawman detector we can estimate the cost of Super*BABAR* by scaling from actual *BABAR* costs, and adding and subtracting additional costs where the designs deviate. The two layer inner pixel tracker is unique to Super*BABAR*. Scaling components of the cost from the even more complex BTeV pixel proposal, we estimate a cost of \$3.8M. The balance of the compact tracking system is built of 2-sided silicon, eliminating the costly drift chamber (saving \$4M). The proposed tracker takes us from *BABAR*'s 9.4K

cm^2 of silicon in 5 layers, to about 100K cm^2 in 7 layers. This is $\sim 1/8$ the area of the GLAST tracker. Adjusting costs for double-sided silicon to $\sim$ \$20 / cm^2, and adding the balance of the readout and mechanics, we estimate the outer 7 layer tracker to cost $\sim$ \$7M. The DIRC at smaller radius has about one half the quartz volume of *BABAR* and replaces the large mechanical structure of the water tank and its $\sim$ 11K phototubes, with a smaller optical interface and smaller number of photodetectors. We assume no net savings (but better performance) in the photodetectors, while the modest savings in quartz ($\sim$ \$1.6M) is offset by the addition of a forward PID system. The calorimeter, if built from a crystal such as LSO, goes from 5.9 m^3 of volume down to about 1.9 m^3, while keeping a similar segmentation of about $\sim$ 14K channels. All construction costs are assumed to be the same, except for the crystals themselves, where three times the present raw material cost ($\sim$ \$20/cc), is assumed for finished LSO. GSO, an excellent alternative with comparable properties, is already available for $\sim$ 15\$/cc. The detector flux return is approximately one half the weight of *BABAR*, but of comparable segmentation, suggesting only a small materials cost reduction. The muon system, being smaller in area but thicker in depth will have similar cost. The coil, while carrying 2x higher current, sits at about one half the *BABAR* radius and being shorter would have only a slightly larger stored energy. Savings in the DAQ from the absence of the drift chamber are offset largely by the more substantial silicon tracking systems. As most other systems have similar readout segmentation (but may require more memory and speed), so the overall cost for electronics are likely to be comparable to *BABAR*. Online DAQ computing costs may increase somewhat to handle the rates. The management costs remain a fixed fraction ($\sim$ 20%) of the total. With these considerations, the straw-man detector is costed at $\sim$ \$121M, in 2001 dollars, assuming US accounting methodology. Including 25% overall contingency and a factor of 1.21 for inflation for the cost in 2008 dollars, the estimated total cost is approximately \$183M.

R&D PROGRAM

The several countries and agencies supporting the ongoing *BABAR* experimental program are likely to be interested in supporting the R&D required for the upgrades described herein. R&D activity has begun; increased support of a variety of activities is required to allow the design of a new detector on the necessary time scale:

- Silicon tracking
  - Low mass pixel devices
  - Low mass double-sided silicon strip devices
  - Low mass mounting, cooling and cabling for these devices
- Alternative approaches to tracking
- Quartz lens readout for the DIRC
- Alternative particle identification systems
- Faster, more rad hard scintillating crystals
  - Appropriate photon detection systems for these crystals
- New technology for muon detection and neutral hadron calorimetry
- Faster electronics and more powerful trigger and data acquisition systems
- More powerful computing for off-line and on-line systems

These items are not all of equal priority. We believe that the tracking, calorimetry and particle ID areas represent the most pressing challenges. We would anticipate, as was done for *BABAR*, to seek independent outside advice in setting up a Super*BABAR* R&D effort.

Schedule

Figure 19 shows the currently planned luminosity acquisition rate for PEP-II, which should reach a total of 600 fb^{-1} in 2007. On the assumption that the PEP-II/*BABAR* complex is shut down in 2008-2009 for the installation of the 10^{36} SuperPEP-II collider and Super*BABAR*, Figure 19 shows the possible integrated luminosity through 2015. The scenario assumes that the collider produces one half its integrated design luminosity in the first year, which equals the performance of PEP-II. With 10 ab^{-1} produced per year, a data sample of 65 ab^{-1}, or more than 2200 times the current PEP-II/*BABAR* sample, would be in hand by 2015.

Conclusions

An asymmetric B Factory at a luminosity of $10^{36}cm^{-2}s^{-1}$ appears to be feasible. Such a collider would produce 2×10^{10} B mesons per Snowmass year, generating a sample fully competitive with, and complementary to, those produced at the new hadron collider experiments. The machine can be built on a time scale that makes this physics capability both relevant and interesting. The physics motivation is quite compelling. Both precision measurements of *CP* asymmetries and searches for rare decays provide unique sensitivity to new physics. New experimental techniques will become possible, using the very large samples of fully reconstructed $B\bar{B}$ pairs. Initial exploration of a detector indicates that the construction of a new experiment capable of doing physics at this unprecedented luminosity is a tractable problem.

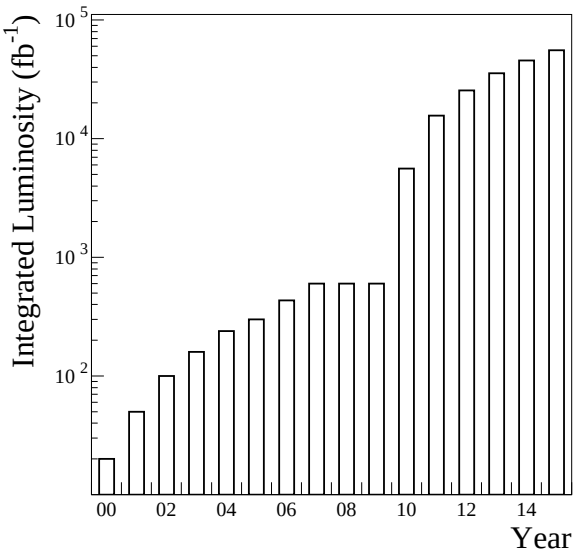

FIG. 19: A plausible scenario for accumulation of integrated luminosity with PEP-II and a 10^{36} collider for the next fifteen years. The integrated luminosity projection for each year is the total expected by July of that year.

Contributors

This report includes contributions from P. Burchat, G. Dubois-Felsmann, G. Eigen, M. Giorgi, D.G. Hitlin, J. Izen, N. Katayama, P. Kim, A. Kronfeld, R. Kutschke, J. Lee, D.W.G.S. Leith, X.C. Lou, M. Piccolo, S. Petrak, I. Peruzzi, B. Ratcliff, S. Robertson, A. Roodman, R. Schindler, J. Seeman, I. Shipsey, A. Soffer, M. Sokoloff, M. Sullivan, W. Wisniewski, H. Yamamoto, S. Yang and C. Young and is based on the work of the P2, E2 and M2 Working Groups of the 2001 DPS Snowmass meeting *The Future of Particle Physics*. Thanks are also due to I. Bigi and Z. Ligeti for illuminating discussions.

References

[1] B. Aubert *et al.* [*BABAR* Collaboration], *Observation of CP violation in the B0 meson system,* hep-ex/0107013.

[2] K. Abe [Belle Collaboration], *Observation of large CP violation in the neutral B meson system,* hep-ex/0107061.

[3] H. Hcker, H. Lacker, S. Laplace and F. Le Diberder , *A New Approach to a Global Fit of the CKM Matrix*, LAL 06/01, hep-ph/0104062. (accepted for publication in EPJ-C).

[4] B. Aubert *et al.* [*BABAR* Collaboration], *Measurement of the decays* $B \to \phi\ K$ *and* $B \to \phi\ K^*$, hep-ex/0105001. R. A. Briere *et al.* [CLEO Collaboration], Phys. Rev. Lett. **86**, 3718 (2001) [hep-ex/0101032].

[5] B. Aubert *et al.* [*BABAR* Collaboration], *Study of CP-violating asymmetries in* $B \to \pi^{\pm}\pi^{\mp}, K^{\pm}\pi^{\mp}$ *decays,* hep-ex/0107074.

[6] M. Gronau and D. London, Phys. Rev. Lett. **65**, 3381 (1990).

[7] M. Gronau and D. Wyler, Phys. Lett. B **265**, 172, (1991).

[8] D. Atwood, I. Dunietz, and A. Soni, Phys. Rev. Lett. **78**, 3257 (1997).

[9] A. Soffer, Phys. Rev. **D60**, 54032 (1999).

[10] R.G. Sachs, Enrico Fermi Institute Report, EFI-85-22 (unpublished) (1985); I. Dunietz and R.G. Sachs, Phys. Rev. **D37**, 3186 (1988); [E: Phys. Rev. **D39**, 3515 (1989)]; I. Dunietz, Phys. Lett. **B427**, 179 (1998); R. Aleksan, I. Dunietz and B. Kayser, Z. Phys. **C54**, 653 (1992).

[11] Cecilia Voena private communication.

[12] D. London, N. Sinha and R. Sinha, Phys. Rev. Lett. **85**, 1807 (2000).

[13] M. Diehl and G. Hiller, hep-ph/0105213 (2001).

[14] J. Lee-Franzini *et al.*, Phys. Rev. Lett. 65 (1990) 2947.

[15] D.M.J. Lovelock *et al.*, (CUSB Collab.), Phys. Rev. Lett. 54 (1985) 377; D. Besson *et al.*, (CLEO Collab.), Phys. Rev. Lett. 54 (1985) 381.

[16] Ph.D. thesis of C.H. Park (1990), S. Nandi (1991) and R. Sangryl (1992) (unpublished).

[17] S. Petrak, Proceedings of the 4th International Conference on B Physics and CP violation (2001).

[18] Y. Keum and U. Nierste, *Phys. Rev.* D **57**, 4282 (1998).

[19] A. Buras and R. Fleischer in *Heavy Flavors II*, eds. A. Buras and M. Lindner (World Scientific, Singapore, 1988) [hep-ph/9704376].

[20] A. Falk and A. Petrov, *Phys. Rev. Lett.* **85**, 252 (2000).

[21] Z. Xing, *Phys. Lett.* B **488**, 162 (2000).

[22] *BTeV Proposal* (2000). *LHC Technical Proposal* LHCC 98/04(1998). N. Harnew, *The B-Phyiscs Potential of LHCb, BTeV, ATLAS, and CMS*, Heavy Flavors 8, (1999).

[23] T.E. Browder *et al* (CLEO), CLNS00-1674, hep-ex/0007057 (2000).

[24] J. Bartelt *et al.* (CLEO), Phys. Rev. Lett. 82, 3746 (1999).

[25] B.H. Behrens *et al.* (CLEO), Phys. Lett. B490, 36 (2000).

[26] B. Aubert *et al.* (*BABAR*) SLAC-PUB-8531, hep-ex/0008053 (2000).

[27] A. Bean *et al.*(CLEO), CBX Note 98-33a (1998).

[28] R. Kowalewski, Presentation at *BABAR* Coll. Meeting, June, 2001.

[29] J. Bartelt *et al*, *Phys. Rev. Lett.* **71**, 4111 (1993).

[30] J. P. Alexander *et al*, *Phys. Rev. Lett.* **77**, 5000 (1996), B. H. Behrens *et al*, *Phys. Rev.* D **61**, 052001 (2000).

[31] A. Falk, Proceedings of the 4th International Conference on B Physics and CP violation (2001).

[32] Z. Ligeti, *Prospects for* V_{cb} *and* V_{ub} talk given at Beyond 10^{34} Physics at a Second Generation *B* Factory, http://www.physics.purdue.edu/10E34.

[33] Aida X. El-Khadra *et al*, hep-ph/0101023.

[34] The *BABAR* Physics Book, SLAC-R-504, 1998.

[35] The CLEO-c Project Description,http:// www.lns.cornell.edu/public/CLEO/spoke/CLEOc.

[36] K. Chetyrkin, M Misiak and M. Munz, Phys. Lett. B **400**, 206 (1997); C. Greub and T. Hurth, Phys. Rev. D **56**, 2934 (1997); A. Buras, A. Kwiatkowski and N. Pott, Nucl. Phys. B **517** 353 (1998).

[37] S. Ahmed *et al.* (CLEO), CLEO-CONF 99-10, hep-

ex/9908022 (1999).
[38] For a review, see C. Greub in Proceedings of the 8th Heavy Flavours Conference, Southampton, hep-ph/9911348 (1999).
[39] E.Thorndike (CLEO), Talk presented at BCP4, Nagoya, 2001.
[40] A. Ali and C. Greub, Phys. Lett. B **361**, 146 (1995); A.L. Kagan and M. Neubert, Eur. Phys. J. **C7**, 5 (1999) .
[41] S. Menke for the *BABAR* Collaboration, Talk presented at EPS 2001, Budapest, July (2001).
[42] A. Ali, L.T. Handoko and D. London, Phys. Rev. D **63**, 014014 (2000).
[43] A. Ali and E. Lunghi, DESY Preprint 01-059, hep-ph/0105200 (2001).
[44] L.T. Handoko, HUPD-9725, hep-ph/9712356 (1997).
[45] G. Burdman, Phys. Rev. D52, 6400 (1995); G. Burdman, MADPH-97-1016, hep-ph/9710550 (1997).
[46] A. Ali, P. Ball, L.T. Handoko and G. Hiller, SLAC-PUB-8269, hep-ph/9910221 (1999).
[47] A.J. Buras *et al.*, TUM-HEP-382, hep-ph/0007313 (2000).
[48] R. Barate *et al.* (ALEPH), Eur.Phys.J. C19, 213 (2001).
[49] J.O. Egg *et al.*, Phys. Lett. B 336, 549 (1994); G.G. Devidze *et al.*, Nucl. Phys. B468, 241 (1998); H. Simma *et al.*, Nucl Phys. B344, 283 (1990).
[50] T. M. Aliev and G. Turan, Phys. Rev. D **48**, 1176 (1993).
[51] B. Aubert, [*BABAR* collaboration] *Search for the decay* $B^0 \to \gamma\gamma$, SLAC-PUB-8931, hep-ex/0107068 (2001).
[52] K. Whisnant *et al.*,Phys. Rev. **D56** 467-468 (1997). Jin Min Yang *et al.*, Phys. Rev. **D56** 5907-5918 (1997).
[53] "R. Barbieri *et al.*, Nucl. Phys. **B445** (1995).
[54] X.C. Lou, *Production of the* $\psi(2S)$ *via Initial State Radiation at the* $\Upsilon(4S)$, To appear in Int. J. of Mod. Phys. **A** (Conference Supplement). E. Solodov, Invited talk presented at Physics at Intermediate Energies, SLAC, Stanford, April 30 - May 2, 2001.
[55] M. Benayoun *et al.*, Modern Phys. Lett. **A14**, 2605 (1999). X.C. Lou *et al.*, Nucl. Phys. **A675**, 2536 (2000).
[56] J. P. Alexander *et al.*, SLAC-PUB-4501, January 1988.
[57] BES Collaboration, J. Z. Bai *et al.*, Phys. Rev. **D62**, 052001 (2000).
[58] E. Eichten *et al.*, Phys. Rev. Lett. **D21**, 203 (1980).
[59] Mark II Collaboration, G. S. Abrams, *et al.*, Phys. Rev. Lett. **44**, 10 (1980).
[60] Y. Funakoshi *et al.*, *KEKB Performance*, EPAC 2000, 28.
[61] J. Seeman *et al.*, *Status Report on PEP-II Performance*, EPAC 2000, 38, and Proceedings of PAC2001.
[62] J. Seeman, *Initial Parameters for a* $10^{36}\,cm^{-2}s{-}1$ *Luminosity* e^+e^- *B Factory*, SLAC-PUB-8787, March 2001.
[63] J. Seeman, *Higher Luminosity B Factories*, Proceedings of PAC2001.
[64] M. Furman, M. Zisman, *Luminosity*, in *Handbook of Accelerator Physics and Engineering*, World Scientific, A. Chao, M. Tigner, eds., 247 (1999).
[65] M. Sullivan, U. Wienands, private communication.
[66] *PEP-II Conceptual Design Report*, SLAC Report 418, June 1993.
[67] B. Parker *et al.*, *Superconducting Magnets for use inside the HERA ep Interaction Regions*, PAC1999 308.
[68] L. Klaisner, private communication.
[69] *BABAR Upgrades Required to Address PEP-II Operations Through* $3 \times 10^{34}\ cm^{-2}s^{-1}$, Report of the Ad-hoc Committee to Investigate Detector Upgrades, April 2000.
`see http://www.slac.stanford.edu/BFROOT /www/Detector/Upgrades/FINALREPORT.pdf`
[70] *Report of the High-Luminosity Background Task Force*, C. Hast, W. Kozanecki, A. Kulikov, T.I. Meyer, S. Petrak, S. Robertson, T. Schietinger, M. Sullivan, J. Va'vra, *BABAR* Note 522, October 2000.
[71] D.W.G.S. Leith, *DryDirc talk at BABAR collaboration meeting*, May (2001).
[72] R. Baggs *et al.*, Nucl. Instrum. Meth **A344**, 547, (1994).